



1 **A critical review of the use of iron isotopes in atmospheric aerosol research**

2

3 Yifan Zhang^{1,5,#}, Rui Li^{2,#}, Zachary B. Bunnell³, Yizhu Chen¹, Guanhong Zhu⁴, Jinlong Ma⁴,

4 Guohua Zhang,¹ Tim M. Conway^{3,*}, Mingjin Tang^{1,*}

5

6 ¹ State Key Laboratory of Advanced Environmental Technology and Guangdong Key
7 Laboratory of Environmental Protection and Resources Utilization, Guangzhou Institute
8 of Geochemistry, Chinese Academy of Sciences, Guangzhou, China

9 ² Department of Environmental Health, School of Public Health, Shanxi Medical University,
10 Taiyuan, China

11 ³ College of Marine Science, University of South Florida, St. Petersburg, Florida, USA

12 ⁴ State Key Laboratory of Isotope Geochemistry, CAS Center for Excellence in Deep Earth
13 Science, Guangzhou Institute of Geochemistry, Chinese Academy of Sciences,
14 Guangzhou, China

15 ⁵ College of Earth and Planetary Sciences, University of Chinese Academy of Sciences, Beijing,
16 China

17

18 * Correspondence: Tim Conway (tmconway@usf.edu), Mingjin Tang (mingjintang@gig.ac.cn)

19

20 # The two authors contributed equivalently to this work.

21

22



23 **Abstract**

24 Deposition of atmospheric aerosols is recognized as a major source of iron (Fe) to the surface
25 oceans, where it acts as a key micronutrient for primary productivity and metabolic functions
26 of marine microbes. Initially, natural desert dust was thought to be the main source of aerosol
27 Fe, albeit largely insoluble; however, in the last few decades, the role of anthropogenic and
28 wildfire sources in providing soluble Fe to aerosols has been increasingly recognized. The
29 stable isotope ratio of Fe ($\delta^{56}\text{Fe}$) has emerged as a potential tracer for discriminating and
30 quantifying sources of aerosol Fe. In this review, we examine the state of the field for using
31 $\delta^{56}\text{Fe}$ as an aerosol source tracer, and constraints on endmember signatures. We begin with an
32 overview of the methodology of $\delta^{56}\text{Fe}$ analysis for aerosol samples. We then describe
33 knowledge of $\delta^{56}\text{Fe}$ endmember signatures of different source materials, and review existing
34 knowledge of the $\delta^{56}\text{Fe}$ signature of ambient aerosols collected from around the globe, and how
35 these measurements can be used to enhance atmospheric Fe deposition modelling. We also
36 examine the various chemical processing mechanisms which might influence $\delta^{56}\text{Fe}$ source
37 signatures of aerosol Fe during its transport in the atmosphere. This review paper is concluded
38 with a perspective on the state of the field and a call for future work. Overall, we find aerosol
39 $\delta^{56}\text{Fe}$ to be a promising tracer, but highlight that greater constraints on both source endmembers
40 and processing mechanisms are needed to fully utilize this tracer.

41

42



43 **1 Introduction**

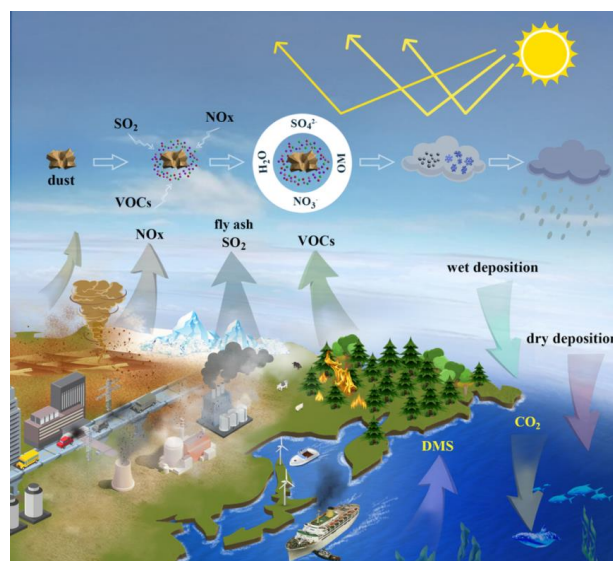
44 Iron (Fe) is the fourth most abundant element in the upper continental crust (UCC), but
45 concentrations of dissolved Fe are very low over much of the surface ocean ($<0.1 \text{ nmol kg}^{-1}$)
46 due to the extremely low solubility of Fe(III) in seawater (Boyd and Ellwood, 2010). Thus, the
47 availability of dissolved Fe may limit marine primary productivity, nitrogen fixation, and
48 ocean-atmosphere carbon exchange over large regions of the surface ocean, especially in High-
49 Nutrient Low Chlorophyll (HNLC) regions (Boyd and Ellwood, 2010; Moore et al., 2013). In
50 early views of the Fe cycle, atmospheric deposition of Fe-bearing aerosols was thought to be
51 the only significant source of dissolved Fe to the surface ocean (Johnson et al., 1997; Tagliabue
52 et al., 2017). However, it is now understood that dissolved Fe is supplied to the oceans by a
53 mixture of external sources that vary in importance by basin, including hydrothermal venting,
54 marine sediment dissolution (both reductive and non-reductive), and atmospheric aerosols
55 (Tagliabue et al., 2017; Conway et al., 2024). Rivers and cryospheric sources may also play a
56 role in some regions. In this view, atmospheric deposition remains a key source of dissolved
57 Fe to the surface ocean, but with great chemical, spatial, and temporal variability that must be
58 understood and characterized.

59 Atmospheric Fe aerosols reaching the oceans were originally considered to be composed
60 only of natural components, derived through the weathering and erosion of UCC materials;
61 indeed, desert dust, mainly emitted from arid and semi-arid regions, is the dominant source of
62 aerosol Fe on the global scale (Jickells et al., 2005). More recently, however, it has been shown
63 that anthropogenic aerosols can account for a large fraction of soluble aerosol Fe despite of
64 their small contribution to total aerosol Fe (Sholkovitz et al., 2009; Ito et al., 2019; Hamilton



65 [et al., 2020a](#); [Rathod et al., 2020](#); [Ito et al., 2021](#); [Chen et al., 2024](#)), meaning that they can play
66 an outsized role in influencing marine primary productivity. Anthropogenic aerosols can
67 include emissions from fossil fuel/biofuel combustion, industry, biomass burning, and
68 transportation ([Sedwick et al., 2007](#); [Sholkovitz et al., 2009](#); [Zhu et al., 2022](#); [Chen et al., 2024](#)).
69 In this article, non-dust sources are referred to as anthropogenic sources in order to highlight
70 the impacts of anthropogenic emission. However, we note that wildfire Fe aerosol, composed
71 of a combination of soil (~64%) and biomass Fe (~36%) ([Hamilton et al., 2022](#); [Bunnell et al.,](#)
72 [2025](#)), is a natural source that may be enhanced by anthropogenic land use and climate change.

73 After emission into the troposphere, natural, anthropogenic, and wildfire aerosols may
74 undergo various chemical and physical processes, which can ‘solubilize’ insoluble Fe minerals
75 to soluble Fe. For example, while Fe in desert dust is ‘insoluble’ with initial solubility
76 (operationally defined as the fraction of total Fe that dissolves) being <0.5% ([Desboeufs et al.,](#)
77 [2005](#); [Shi et al., 2011](#); [Oakes et al., 2012](#); [Li et al., 2022](#)), several chemical processes can
78 promote dissolution of insoluble Fe, among which acid processing (i.e. proton-promoted
79 dissolution) is likely the most important ([Meskhidze et al., 2003](#); [Shi et al., 2012](#); [Baker et al.,](#)
80 [2021](#); [Zhang et al., 2023](#)). Indeed, many studies ([Baker and Jickells, 2006](#); [Kumar et al., 2010](#);
81 [Sholkovitz et al., 2012](#); [Mahowald et al., 2018](#); [Sakata et al., 2022](#)) have shown that when
82 compared to desert dust, Fe solubility can be much higher for ambient aerosol particles
83 collected over the oceans, suggesting that other sources (e.g., anthropogenic Fe) or atmospheric
84 processes contribute significantly to soluble aerosol Fe in the troposphere (and for later
85 deposition to the surface oceans).



86

87 **Figure 1.** Emission, transport, processing and deposition of aerosol Fe. VOCs: volatile organic
 88 compounds; OM: organic materials; DMS: dimethyl sulfide.

89

90 Figure 1 depicts emission, transport, processing, and deposition of aerosol Fe. Observed
 91 variability in aerosol Fe flux, composition, and solubility can, in principle, be explained by a
 92 mix of different source emissions and secondary processing in the atmosphere. However, each
 93 type of Fe source exhibits large temporal and spatial variations at the local-global scale, and
 94 thus it remains difficult to quantitatively disentangle their contributions to a sample or location.
 95 Enrichment factors, correlation analysis, and factor analysis (such as positive matrix
 96 factorization) are approaches that have been used for source appointment of total and soluble
 97 aerosol Fe (Chuang et al., 2005; Sedwick et al., 2007; Sholkovitz et al., 2009; Buck et al., 2010;
 98 Desboeufs et al., 2018; Marsay et al., 2022; Zhu et al., 2022; Sakata et al., 2023; Zhang et al.,
 99 2023; Chen et al., 2024; Zhang et al., 2024). However, enrichment factors of other
 100 ‘anthropogenically-derived’ elements (e.g., Cd, Pb, Ni, and Zn) may not always be indicative



101 of anthropogenic Fe (Chester et al., 1993; Shelley et al., 2015), and a consensus has not been
102 reached on either the relative contribution of various sources to soluble aerosol Fe or the factors
103 which control aerosol Fe solubility (Mahowald et al., 2018; Meskhidze et al., 2019; Baker et
104 al., 2021). Single particle analysis can also be very useful for source identification of aerosol
105 Fe in individual particles (Li et al., 2017; Zhu et al., 2020; Liu et al., 2022); nevertheless, it can
106 only examine a limited number of aerosol particles, and thus may not be able to provide
107 quantitative information on the source of Fe for an aerosol sample which typically consists of
108 numerous particles.

109 One tracer that shows recent promise in source quantification of total and soluble Fe
110 within aerosols themselves is the isotopic composition of Fe ($\delta^{56}\text{Fe}$). During the last two
111 decades, this parameter has been measured both in marine source materials (Beard et al., 2003a)
112 and later seawater itself (De Jong et al., 2007), providing very useful information for
113 disentangling the marine Fe cycle (Fitzsimmons and Conway, 2023). The developing
114 application of $\delta^{56}\text{Fe}$ to aerosols has also been shown to be a promising way to differentiate
115 sources of total and soluble Fe in atmospheric aerosols and to quantify their relative importance
116 (Majestic et al., 2009b; Mead et al., 2013; Conway et al., 2019; Kurisu et al., 2021). Wang et
117 al. (2022) briefly summarized recent advances in isotopic compositions of aerosol Fe, and
118 utilized a Bayesian isotopic mixing model (MIXSIAR) to re-evaluate the sources of aerosol Fe
119 based on Fe isotopic data reported in literature. Wei et al. (2024) compiled a global dataset of
120 aerosol Fe isotope measurements, and identified coal combustion as the major anthropogenic
121 source of aerosol Fe by using MIXSIAR to re-analyze the data they compiled.

122 Here, we review the application of Fe isotopic analysis to atmospheric aerosol research in



123 a comprehensive and critical manner. We summarize the current consensus, underscore existing
 124 discrepancies, and uncertainties/unknowns, as well as outline future research priorities required
 125 to improve the use of Fe isotopic analysis in tracing sources of atmospheric aerosol Fe and
 126 understanding processes that influence its solubility.

127 **2 Introduction to Fe isotopes and their analysis**

128 **2.1 Natural Fe isotopes**

129 Fe has four stable isotopes which occur naturally, namely ^{54}Fe (5.84%), ^{56}Fe (91.76%),
 130 ^{57}Fe (2.12%) and ^{58}Fe (0.28%). Fe isotopic compositions are typically reported in δ values, as
 131 given in Eq. (1) (Beard and Johnson, 2004; Dauphas and Rouxel, 2006):

$$132 \quad \delta^x\text{Fe}(\text{‰}) = \left[\frac{(^x\text{Fe}/^{54}\text{Fe})_{\text{sample}}}{(^x\text{Fe}/^{54}\text{Fe})_{\text{standard}}} - 1 \right] \times 1000 \quad (1)$$

133 where x is 56, 57 or 58. While some studies report $\delta^{57}\text{Fe}$, the convention is to report $\delta^{56}\text{Fe}$,
 134 which allows for easy inter-comparability. Here, we use $\delta^{56}\text{Fe}$ values, although we note that
 135 $\delta^{57}\text{Fe}$ can be converted to $\delta^{56}\text{Fe}$ by dividing $\delta^{57}\text{Fe}$ values by 1.475. Fe isotopic data is also
 136 typically reported relative to the IRMM-014 standard, although some early workers have used
 137 other standards (Beard and Johnson, 2004). In this article we use $\delta^{56}\text{Fe}$ values relative to
 138 IRMM-014, and for the ease of the reader, have converted published values that were expressed
 139 relative to other standards.

140 **2.2 Fe isotopic analysis**

141 Historically, $\delta^{56}\text{Fe}$ measurements have been made by either multi-collector Thermal
 142 Ionization Mass spectrometry (MC-TIMS) or multi-collector Inductively Coupled Plasma
 143 Mass Spectrometry (MC-ICP-MS). In early works, TIMS was combined with the double-spike
 144 technique, yielding precision of $\pm 0.5\text{‰}$ (2σ) (Beard and Johnson, 1999; Beard and Johnson,



145 2004). However, the TIMS-based method, which does not suffer from isobaric interferences,
146 requires a very long time for each measurement (usually 4-8 hours), and has low Fe ionization
147 efficiency (Beard et al., 2003b), variable mass bias, and relatively low precision (0.5‰)
148 compared to natural variability (typically 1-2‰) in open ocean seawater (Dauphas and Rouxel,
149 2006; Fitzsimmons and Conway, 2023).

150 The development of MC-ICP-MS, with high ionization efficiency, short analysis time per
151 measurement, and higher precision ($<0.1\text{‰}$) than TIMS, was crucial to application of $\delta^{56}\text{Fe}$ to
152 natural materials (Beard and Johnson, 2004; Zhang et al., 2022). Currently the precision of
153 $\delta^{56}\text{Fe}$ measurements via MC-ICP-MS can reach ± 0.02 to $\pm 0.05\text{‰}$ (2σ) (De Jong et al., 2007;
154 Zhu et al., 2018; Conway et al., 2019), around an order of magnitude better than TIMS;
155 therefore, MC-ICP-MS has been much more widely used for Fe isotopic analysis.

156 Drawbacks of MC-ICP-MS are the need of correction for rapid changes in mass bias, and
157 that measurements can be compromised by isobaric and polyatomic spectral interferences that
158 must be dealt with using several approaches (Beard et al., 2003b; Beard and Johnson, 2004).
159 For example, mass-bias must be corrected for using standard-sample bracketing and/or double-
160 spike techniques, and samples must be cleanly purified from interfering isobars (Cr and Ni)
161 and matrix elements (e.g., Ca). A further non-trivial challenge of using MC-ICP-MS is the
162 presence of distinct polyatomic argide interferences (e.g., ArO and ArN) that arise on masses
163 of ^{54}Fe , ^{56}Fe , ^{57}Fe and ^{58}Fe from combination of the plasma gas and solvent matrix, and can be
164 larger than the Fe mass of interest (Weyer and Schwieters, 2003). Furthermore, while elemental
165 isobars and polyatomic interferences, such as Ni, Cr, and CaO , can be dealt with by purification
166 and/or correction, argides must be dealt with by changing instrumental conditions or using



167 ‘high’ resolution instruments which can sufficiently resolve Fe peaks from argide interferences
168 ([Weyer and Schwieters, 2003](#)).

169 The minimum mass of Fe required for isotopic analysis by MC-ICP-MS depends on
170 several factors, including the procedural blank, analytical uncertainty, and minimum
171 concentration at which an accurate isotope ratio can be obtained. As MC-ICPMS Neptune Fe
172 signal intensity decreases, analytical internal standard error (SE) increases relatively
173 predictably ([John and Adkins, 2010](#); [Conway et al., 2013](#)).

174 Thus, assuming no inaccuracy at lower concentrations, a minimum mass depends on
175 instrumental signal sensitivity (volts per ng/g) and the minimum acceptable uncertainty for a
176 sample (e.g., <0.2‰ for Fe). As an example, at the University of South Florida (USF), with a
177 typical sensitivity of 0.1-0.15 V on ^{56}Fe per ng of Fe, we are typically able to achieve acceptable
178 2SE (<0.15‰) in solutions at concentrations of 10 ng/g, a concentration that is >20-40 times
179 of our chemistry procedural blank ([Sieber et al., 2021](#)). This concentration can be achieved by
180 dissolving 5 ng Fe in 0.5 mL solution. Furthermore, we found that at concentrations below 1V
181 on ^{56}Fe , inaccuracies in our measurement of the zero standard begin to occur. In both cases, 5
182 ng Fe can therefore be considered an absolute minimum mass for analysis. However, 20-100
183 ng Fe provides isotopic ratios with smaller uncertainty (<0.1‰), approaching the analytical
184 precision at USF (0.06‰). Similarly, [Kurisu et al. \(2024\)](#) used a minimum of 25 ng Fe to obtain
185 Fe isotopic data from aerosol samples with suitable uncertainties, but they preferred ~100 ng
186 where possible. Such precision is often essential for resolving variability between aerosol
187 samples.

188 A further consideration for aerosol samples that often include significant filter or



189 digestion blanks is the blank isotopic composition should be established (and subtracted,
190 weighed by concentration, from samples) and/or the effect of blanks minimized by having large
191 sample to blank ratios.

192 **3 Application of Fe isotopic analysis in aerosol research**

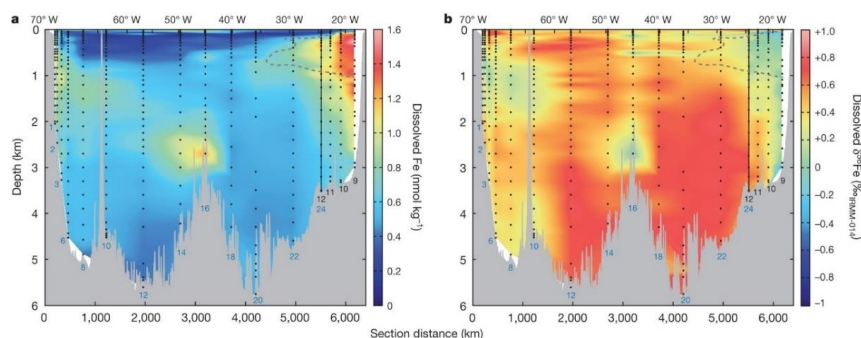
193 In this section we first present a few examples to illustrate how Fe isotopic analysis may
194 help constrain sources of dissolved Fe to the ocean (Section 3.1). After that, we review isotopic
195 compositions of aerosol Fe from relevant sources (Section 3.2), Fe isotopic composition of
196 ambient aerosols (Section 3.3), modeling studies of isotopic compositions of ambient aerosol
197 Fe (Section 3.4), and Fe isotopic fractionation induced by chemical processing (Section 3.5).

198 **3.1 Application of Fe isotopic analysis to marine source attribution**

199 Since the first successful application of $\delta^{56}\text{Fe}$ to seawater samples in 2007-2010 ([De Jong](#)
200 [et al., 2007](#); [Lacan et al., 2008](#); [John and Adkins, 2010](#)), Fe isotopic analysis has been
201 increasingly deployed in investigating marine biogeochemistry over the last decade,
202 significantly increasing our knowledge of sources and cycles of Fe in the ocean ([Conway et al.,](#)
203 [2021](#); [Fitzsimmons and Conway, 2023](#)), with a precision of +0.05 to +0.07‰. As this article is
204 focused on atmospheric aerosols, we do not intend to provide a comprehensive review of the
205 application of Fe isotopes to marine biogeochemistry; instead, we present a few examples of
206 relevant ocean observational and modeling studies to illustrate how $\delta^{56}\text{Fe}$ may help constrain
207 sources of dissolved Fe to the ocean, focusing on aerosol deposition case studies. For a more
208 comprehensive discussion of the advances in using $\delta^{56}\text{Fe}$ to interrogate the marine Fe cycle in
209 recent years, we instead point the reader to [Fitzsimmons and Conway \(2023\)](#).



210 Although a few marine $\delta^{56}\text{Fe}$ water column profiles had been measured by 2012 (Lacan
 211 et al., 2010; Radic et al., 2011; John and Adkins, 2012), the first ocean ‘section’ of $\delta^{56}\text{Fe}$ came
 212 in 2014 when Conway and John (2014) reported dissolved Fe and $\delta^{56}\text{Fe}$ in 510 seawater
 213 samples at 17 stations along the U. S. GEOTRACES GA03 section of the subtropical North
 214 Atlantic Ocean from Woods Hole to Mauritania (Figure 2). A range of $\delta^{56}\text{Fe}$ values, spanning
 215 from -1.35‰ to +0.8‰, were observed at different regions along this section, reflecting
 216 different sources of dissolved Fe. Most strikingly, much of this transect was characterized by
 217 $\delta^{56}\text{Fe} > +0.1\text{‰}$, heavier than known sources of Fe to the ocean at the time and attributed to the
 218 net dissolution of atmospheric dust (John and Adkins, 2012; Conway and John, 2014). Further,
 219 by assigning endmember compositions to each identified Fe source (dust, hydrothermal venting,
 220 and sediments), two component mixing was used to quantitatively constrain sources across the
 221 basin (Conway and John, 2014): Saharan dust aerosol was found to be the dominant source for
 222 dissolved Fe along this section (71-87%), with lesser contribution from non-reductive and
 223 reductive sedimentary dissolution (10-19% and 1-4%), and hydrothermal venting (2-6%).
 224 However, that study was not able to use $\delta^{56}\text{Fe}$ as a source constraint at the very surface, due to
 225 potential influence of biological uptake, and/or anthropogenic aerosols or sediment sources
 226 (Conway and John, 2014; Conway et al., 2019).





228 **Figure 2.** Concentrations (a) and $\delta^{56}\text{Fe}$ values (b) of dissolved Fe in seawater at different depth
229 along a section of the North Atlantic Ocean from Mauritania and Woods Hole. Station numbers
230 are shown in blue or black. Reproduced with permission from [Conway and John \(2014\)](#).

231

232 A second example of where $\delta^{56}\text{Fe}$ has been useful for informing our understanding of
233 atmospheric Fe deposition comes from the North Pacific, where [Pinedo-González et al. \(2020\)](#)
234 analyzed surface seawater samples collected along a latitudinal section at 158°W (from 25 to
235 42°N) in May 2017. Surface dissolved Fe concentrations peaked at ~35°N and were lower at
236 southern and northern ends of this transect, and a similar latitudinal pattern was observed for
237 dissolved Pb, attributed to deposition of anthropogenic aerosol of both elements. Moreover, the
238 lowest $\delta^{56}\text{Fe}$ values (from -0.65‰ to -0.23‰) were observed coincident with the highest
239 concentrations of dissolved Fe ([Pinedo-González et al., 2020](#)), consistent with studies that
240 showed anthropogenic aerosols to be isotopically light ([Kurusu et al., 2016a](#); [Conway et al.,](#)
241 [2019](#)). Using their $\delta^{56}\text{Fe}$ data and estimates of anthropogenic endmember composition, [Pinedo-](#)
242 [González et al. \(2020\)](#) suggested anthropogenic aerosol to be a significant source (21-59%) of
243 dissolved Fe in surface seawater between 35 and 40 °N, at least during the high dust season.
244 However, other studies of the North Pacific have shown that the primary $\delta^{56}\text{Fe}$ signature of
245 aerosol deposition is likely to be strongly attenuated by in situ processing and biological uptake
246 ([Kurusu et al., 2024](#)).

247 Measurements of surface $\delta^{56}\text{Fe}$ may therefore be useful in investigating atmospheric
248 addition of dissolved Fe, but further work is needed to understand the effect of multiple
249 biogeochemical processes which occur upon dissolution in the ocean. Global biogeochemical



250 modeling may prove useful here, with recent work by König et al. (2021) incorporating Fe
 251 isotopes into a global model. This study (König et al., 2021) and a follow-up study focused on
 252 the North Pacific (König et al., 2022) found that both external source signatures and
 253 fractionation during Fe complexation by organic ligands and uptake by phytoplankton were
 254 needed to reproduce oceanic deposition patterns, and that the dissolved $\delta^{56}\text{Fe}$ in surface waters
 255 did not simply follow the footprint of atmospheric deposition.

256 **3.2 Fe isotopic compositions of aerosols from relevant sources**

257 In this section we review Fe isotopic compositions of desert dust (Section 3.2.1), raw
 258 materials relevant for anthropogenic emission and biomass burning (Section 3.2.2), and
 259 anthropogenic and biomass burning aerosols (Section 3.2.3). In addition, Table S1 summarizes
 260 key results reported by previous studies.

261 **3.2.1 Desert dust**

262 Here we discuss Fe isotopic compositions of desert dust reported by previous work.
 263 Instead of providing a complete literature survey, we review some representative studies. Fe
 264 isotopic compositions appear to be rather homogeneous for UCC, and $\delta^{56}\text{Fe}$ values fall into a
 265 narrow range centered at around $+0.09 \pm 0.10\text{‰}$ (Beard et al., 2003b; Beard and Johnson, 2004;
 266 Poitrasson, 2006).

267 The average $\delta^{56}\text{Fe}$ values were determined to be $+0.13 \pm 0.06\text{‰}$ and $+0.12 \pm 0.07\text{‰}$ for loess
 268 ($n = 10$) and soil samples ($n = 10$) collected from various locations around the world,
 269 respectively (Beard et al., 2003a). Waeles et al. (2007) measured Fe isotopic compositions of
 270 Chinese and Australian desert dust samples, and the average $\delta^{56}\text{Fe}$ were determined to be
 271 $+0.08 \pm 0.04\text{‰}$ ($n = 8$) for total Fe and -0.06‰ ($n = 2$) for soluble Fe, suggesting that the isotopic



272 composition of soluble Fe in acetate buffer is similar to total Fe. [Majestic et al. \(2009b\)](#)
 273 measured Fe isotopic compositions of road dust and agricultural soil in Phoenix (Arizona,
 274 USA), and $\delta^{56}\text{Fe}$ values were found to range from -0.10‰ to +0.14‰ for road dust and from -
 275 0.07‰ to 0.04‰ for agricultural soil, both similar to desert dust. In another study ([Mead et al.,](#)
 276 [2013](#)), average $\delta^{56}\text{Fe}$ was reported to be 0.09 ± 0.04 ‰ for three dust samples, namely ATD,
 277 Saharan dust and San Joaquin soil (SRM1709). The $\delta^{56}\text{Fe}$ values were determined to be -
 278 0.04 ± 0.10 ‰, -0.05 ± 0.06 ‰ and 0.21 ± 0.05 ‰ for ATD, China loess and Xinjiang dust ([Li et](#)
 279 [al., 2022](#)), with the average being 0.04 ± 0.15 ‰.

280 The $\delta^{56}\text{Fe}$ values were found to range from +0.06‰ to 0.12‰ for loess and paleosol
 281 samples ($n = 32$) from the China Loess Plateau, with the average being 0.09 ± 0.03 ‰ ([Gong et](#)
 282 [al., 2017](#)). [Chen et al. \(2020\)](#) analyzed isotopic compositions of HCl-leachable Fe in desert dust
 283 samples ($n = 10$) from different deserts in northern China: one sample from northeastern China
 284 exhibited low $\delta^{56}\text{Fe}$ (-0.23‰), while $\delta^{56}\text{Fe}$ showed very small variation and had an average
 285 value of -0.09 ± 0.07 ‰ for the other nine samples.

286 One may conclude from previous work that Fe isotopic compositions of desert dust are
 287 very similar to UCC, and most of $\delta^{56}\text{Fe}$ values fall into a small range (-0.1 to +0.19‰) with an
 288 average value of around +0.09‰. Furthermore, soluble Fe from desert dust appears to be
 289 isotopically similar to total Fe ([Waeles et al., 2007](#); [Chen et al., 2020](#)). We note from a recent
 290 synthesis that isotopic compositions of Fe in soil can range from -0.2 to +0.95‰ ([Johnson et](#)
 291 [al., 2020](#)), showing more variability than in dust, and reflecting the effects of organic matter,
 292 mineralogy, and chemistry.

293 3.2.2 Raw materials relevant for anthropogenic emission and biomass burning



294 Before we discuss isotopic compositions of aerosol Fe from anthropogenic emission and
295 biomass burning, it is helpful to review Fe isotopic compositions of relevant raw materials,
296 including iron ore, fossil fuel, biomass, and so on.

297 Iron deposits have been found to display very large variations in Fe isotopic compositions
298 (Johnson et al., 2003; Lobato et al., 2023), with $\delta^{56}\text{Fe}$ spanning from below -1.5 to around
299 +2.0‰. The $\delta^{56}\text{Fe}$ value was determined to be $+0.28 \pm 0.13$ ‰ for one commercial gasoline
300 sample in Japan (Kurusu et al., 2016b). To our knowledge, Fe isotopic compositions have not
301 been reported for other important fossil fuels.

302 Guelke and Von Blanckenburg (2007) measured isotopic compositions of Fe in higher
303 plants and plant-available Fe in soils where these plants were grown. Compared to plant-
304 available Fe in soils, Fe in strategy I plants were isotopically lighter by up to -1.6‰ (Guelke
305 and Von Blanckenburg, 2007), and younger parts in these plants were more depleted in heavy
306 Fe. Fe in strategy II plants was isotopically heavier by about +0.2‰ than plant-available Fe in
307 soils (Guelke and Von Blanckenburg, 2007), and all the parts in these plants had nearly the
308 same isotopic composition.

309 In a later study (Kurusu and Takahashi, 2019), average $\delta^{56}\text{Fe}$ were reported to be
310 $+0.08 \pm 0.10$ ‰ for reed and $+0.09 \pm 0.03$ ‰ for reed burning residual ash, both similar to that for
311 nearby soil ($+0.04 \pm 0.20$ ‰). As a result, Kurusu and Takahashi (2019) suggested that biomass
312 burning could not explain isotopically lighter Fe observed for ambient aerosols.

313 Kubik et al. (2021) surveyed Fe isotopic compositions of biological samples and found
314 that in general Fe in strategy I plants is isotopically lighter than strategy II plants. For example,
315 $\delta^{56}\text{Fe}$ in stems ranged from -0.72 to -0.08‰ for strategy I plants, and from -1.28‰ to +0.25‰



for strategy II plants; $\delta^{56}\text{Fe}$ in leaves ranged from -1.04 to +0.23‰ for strategy I plants, and from -1.20 to 0.24‰ for strategy II plants; $\delta^{56}\text{Fe}$ in seeds ranged from -1.52 to +0.15‰ for strategy I plants, and from -1.00 to +0.16‰ for strategy II plants. While various organic materials have been analyzed for $\delta^{56}\text{Fe}$ (Guelke and Von Blanckenburg, 2007; Guelke-Stelling and Von Blanckenburg, 2012; Kurisu and Takahashi, 2019; Kubik et al., 2021), the isotopic signature for biomass burning as a source of ambient aerosol Fe remains unconstrained. Additionally, recent work (Hamilton et al., 2022) showed that soil Fe, rather than biomass Fe, dominates aerosols produced in large scale biomass burning events (wildfires).

In summary, $\delta^{56}\text{Fe}$ varied greatly from below -1.5‰ to around +2.0‰ for iron ore; no conclusions can be drawn on $\delta^{56}\text{Fe}$ for fossil fuel, as observational data are very rare; compared to desert dust, $\delta^{56}\text{Fe}$ values can be much lower for plants (and especially strategy I plants). However, it should be pointed out that $\delta^{56}\text{Fe}$ values may not be identical for aerosol particles emitted and their relevant raw materials because Fe isotopic fractionation may occur during combustion and industrial processes (e.g., iron smelting).

3.2.3 Anthropogenic aerosols

Average $\delta^{56}\text{Fe}$ were determined by Beard et al. (2003a) to be $0.00 \pm 0.03\text{‰}$ ($n = 2$) for urban dust (NIST 1649a). Mead et al. (2013) reported the average $\delta^{56}\text{Fe}$ to be $+0.35 \pm 0.23\text{‰}$ ($n = 3$) for coal fly ash and $+0.30 \pm 0.17\text{‰}$ ($n = 4$) for oil fly ash; in addition, $\delta^{56}\text{Fe}$ values were measured to be $-0.03 \pm 0.13\text{‰}$ for one diesel particulate matter sample (NIST 1650b) and $0.01 \pm 0.12\text{‰}$ for one urban dust sample (NIST 1649a) (Mead et al., 2013). In another study (Li et al., 2022), $\delta^{56}\text{Fe}$ were found to be in the range of $+0.05 \pm 0.08\text{‰}$ to $+0.75 \pm 0.01\text{‰}$ for three



337 coal fly ash samples (average: $+0.33 \pm 0.37\text{‰}$) and $+0.10 \pm 0.08\text{‰}$ for one municipal waste fly
338 ash (BCR-176R).

339 In one of the largest steelworks in Europe, $\delta^{56}\text{Fe}$ values displayed larger variations for
340 enriched iron ores, ranging from -0.16 ± 0.07 to $+1.19 \pm 0.14\text{‰}$ (Flament et al., 2008); for
341 comparison, $\delta^{56}\text{Fe}$ values were found to be in the range of $+0.53 \pm 0.14$ to $+0.80 \pm 0.06\text{‰}$ for
342 sintering fly ash and $+0.08 \pm 0.24\text{‰}$ for steelwork fly ash. Flament et al. (2008) further
343 suggested that $\delta^{56}\text{Fe}$ values reported for sintering and steelwork fly ash fell into the range of
344 their raw materials (enriched iron ores), implying no significant Fe isotopic fractionation during
345 steel processes; however, as both enriched iron ores and fly ash displayed large variation in
346 $\delta^{56}\text{Fe}$, this conclusion could be uncertain.

347 In a parking garage, the average $\delta^{56}\text{Fe}$ was reported to be $+0.15 \pm 0.03\text{‰}$ for coarse
348 particles ($>2.5 \mu\text{m}$) (Majestic et al., 2009a), similar to that ($+0.18 \pm 0.03\text{‰}$) for fine particles
349 ($<2.5 \mu\text{m}$) but slightly larger than that for desert dust. Furthermore, $\delta^{56}\text{Fe}$ were found to be
350 $+0.19\text{‰}$ for metallic brake pads, and ranged from $+0.42$ to $+0.61\text{‰}$ for ceramic brake pads,
351 from -0.08 to $+0.12\text{‰}$ for tire thread, and from $+0.04$ to $+0.11\text{‰}$ for waste oil (Majestic et al.,
352 2009a).

353 The aforementioned studies measured isotopic compositions of total Fe in urban dust
354 (Beard et al., 2003a; Mead et al., 2013), coal fly ash (Mead et al., 2013; Li et al., 2022), oil fly
355 ash (Mead et al., 2013), diesel particulate matter (Mead et al., 2013), municipal waste fly ash
356 (Li et al., 2022), sintering and steelwork fly ash (Flament et al., 2008), brake pads, tire thread
357 and waste oil of vehicles (Majestic et al., 2009a), and aerosol particles collected in a parking
358 garage (Majestic et al., 2009a). The reported $\delta^{56}\text{Fe}$ values, which show large variations, are



359 similar to or larger than that for desert dust, and isotopically lighter Fe has hardly been found
360 in these studies (Beard et al., 2003a; Flament et al., 2008; Majestic et al., 2009a; Mead et al.,
361 2013; Li et al., 2022).

362 In contrast, Kurisu et al. (2016b) observed much lower $\delta^{56}\text{Fe}$ for anthropogenic emissions,
363 as discussed below. For total Fe in aerosol particles collected in a tunnel in Japan, coarse
364 particles ($>1\ \mu\text{m}$) had $\delta^{56}\text{Fe}$ close to UCC while fine particles ($<1\ \mu\text{m}$) exhibited much lower
365 $\delta^{56}\text{Fe}$ (as low as -3.2‰) (Kurisu et al., 2016b). Furthermore, $\delta^{56}\text{Fe}$ were measured to be -
366 $0.08\pm0.09\text{‰}$, $-0.10\pm0.03\text{‰}$, and $-0.66\pm0.09\text{‰}$ for total Fe in bottom and fly ash of an
367 incinerator in Japan and total suspended particles (TSP) collected close to its chimney, and -
368 $0.34\pm0.14\text{‰}$, $-1.97\pm0.18\text{‰}$, and $-1.25\pm0.10\text{‰}$ for soluble Fe (leached using 1 mol/L HCl),
369 respectively (Kurisu et al., 2016b). Compared to bottom and fly ash, total Fe in TSP exhibited
370 much lower $\delta^{56}\text{Fe}$ values; in addition, soluble Fe was isotopically lighter than total Fe. The
371 following mechanism was proposed to explain their observation (Kurisu et al., 2016b): the
372 evaporation-condensation process during combustion produced isotopically lighter but more
373 soluble Fe which was enriched in fly ash and specially in emitted aerosol particles, while most
374 Fe in bottom ash did not undergo evaporation-condensation. This argument may explain the
375 discrepancies between the work by Kurisu et al. (2016b) and other studies (Beard et al., 2003a;
376 Flament et al., 2008; Majestic et al., 2009a; Mead et al., 2013; Li et al., 2022), and can also
377 explain isotopic compositions of total and soluble Fe in ambient aerosols reported by field
378 studies (Majestic et al., 2009b; Mead et al., 2013; Kurisu et al., 2016a; Conway et al., 2019;
379 Kurisu et al., 2019; Kurisu et al., 2021; Zuo et al., 2022).

380 3.2.4 Discussion



381 Since the work by [Beard et al. \(2003a\)](#), there have been a small number of studies which
382 measured isotopic compositions of aerosol Fe from relevant sources. As discussed in Section
383 3.2.1, $\delta^{56}\text{Fe}$ endmember values have been reasonably well understood for total Fe in desert dust,
384 being similar to UCC. On the other hand, previous studies which measured $\delta^{56}\text{Fe}$ endmember
385 values for anthropogenic aerosols report a range of isotopic compositions ([Beard et al., 2003a](#);
386 [Flament et al., 2008](#); [Majestic et al., 2009a](#); [Mead et al., 2013](#); [Kurusu et al., 2016b](#); [Kurusu and](#)
387 [Takahashi, 2019](#); [Li et al., 2022](#)), and the endmember values remain poorly constrained for
388 wildfire aerosols ([Bunnell et al., 2025](#)). In general, the number of relevant studies of
389 endmembers is very small, and the number of samples covered by each of these studies is also
390 limited; furthermore, compared to total Fe, $\delta^{56}\text{Fe}$ endmember values of soluble Fe have been
391 much less examined.

392 The lack of reliable $\delta^{56}\text{Fe}$ endmember values for total and soluble Fe in non-desert-dust
393 aerosols does limit the use of $\delta^{56}\text{Fe}$ in tracing and constraining the sources of total and soluble
394 Fe in ambient aerosols. However, we note that the existing studies show much promise.
395 Therefore, we strongly recommend additional measurements of $\delta^{56}\text{Fe}$ endmember values for
396 total and soluble Fe in non-desert-dust aerosols (aerosols emitted from fossil fuel combustion,
397 biomass burning and metal smelting, for example). In addition, it is very important to continue
398 to explore the dependence of $\delta^{56}\text{Fe}$ endmember values on particle size, as some previous studies
399 suggested that Fe was isotopically lighter in fine particles when compared to coarse particles
400 ([Mead et al., 2013](#); [Kurusu et al., 2016b](#); [Kurusu et al., 2019](#); [Kurusu et al., 2024](#); [Bunnell et al.,](#)
401 [2025](#)).

402 3.3 Fe isotopic composition of ambient aerosols



403 Table S2 summarizes previous studies which measured Fe isotopic compositions of
404 ambient aerosols. Studies published before 2016 and since 2016 are reviewed in Sections 3.3.1
405 and 3.3.2, respectively. Large variations in $\delta^{56}\text{Fe}$ have been reported for ambient aerosols: $\delta^{56}\text{Fe}$
406 ranged from -3.53 to +0.48‰ for total aerosol Fe, and from -4.46 to +0.47‰ for soluble aerosol
407 Fe; by comparison, only a small range of $\delta^{56}\text{Fe}$ (-0.1 to +0.2‰) has been reported for desert
408 dust, with an average value of +0.1‰.

409 3.3.1 Studies published prior to 2016

410 [Beard et al. \(2003a\)](#) reported the first measurement of isotopic signatures of ambient
411 aerosol Fe. The average $\delta^{56}\text{Fe}$ of total Fe were determined to be -0.04 ± 0.04 ‰ for the two TSP
412 samples collected close to the Gobi desert and $+0.11 \pm 0.07$ ‰ for the 12 TSP samples collected
413 at a site in the northwest Pacific ([Beard et al., 2003a](#)), both similar to desert dust.

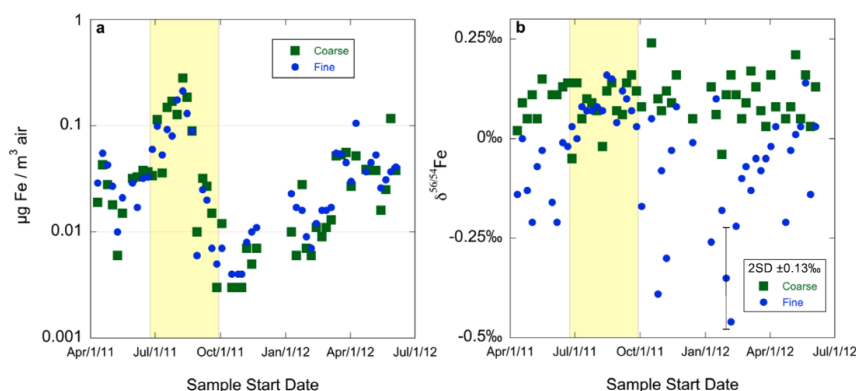
414 [Waeles et al. \(2007\)](#) measured Fe isotopic compositions of aerosols collected over the
415 Atlantic and in Barbados, and the average $\delta^{56}\text{Fe}$ was determined to be $+0.04 \pm 0.09$ ‰ for total
416 aerosol Fe and $+0.13 \pm 0.18$ ‰ for soluble aerosol Fe. No significant difference in isotopic
417 composition was observed between total and soluble aerosol Fe ([Waeles et al., 2007](#)), although
418 desert dust aerosol could be greatly aged at Barbados which is ~4000 km away from the dust
419 region.

420 At an urban site severely affected by a large steel metallurgy plant in France, total aerosol
421 Fe was found to have an average $\delta^{56}\text{Fe}$ of $+0.14 \pm 0.11$ ‰ ([Flament et al., 2008](#)), similar to desert
422 dust. For three aerosol samples collected over the western equatorial Pacific, $\delta^{56}\text{Fe}$ of total Fe
423 ranged from +0.27 to +0.38‰ with an average value of $+0.33 \pm 0.11$ ‰ ([Labatut et al., 2014](#)),
424 slightly higher than desert dust.



425 [Majestic et al. \(2009b\)](#) investigated isotopic compositions of total Fe in PM_{2.5} and PM₁₀
 426 simultaneously collected at a mixed suburban/agricultural site (Phoenix, Arizona, USA). The
 427 first group of PM₁₀ samples had $\delta^{56}\text{Fe}$ values (centered at around +0.03‰) similar to desert
 428 dust, while the other group of PM₁₀ samples exhibited lower $\delta^{56}\text{Fe}$ values (centered at -0.18‰),
 429 indicating different Fe sources for the two groups of PM₁₀ samples ([Majestic et al., 2009b](#)).
 430 Furthermore, the $\delta^{56}\text{Fe}$ values of total Fe were substantially lower in PM_{2.5} samples (average:
 431 $-0.42 \pm 0.14\text{‰}$) than PM₁₀ samples (average: $-0.07 \pm 0.11\text{‰}$) ([Majestic et al., 2009b](#)), and the
 432 difference was correlated with concentrations (in PM_{2.5}) of anthropogenically dominated
 433 elements (such as Pb, V and Cr). Therefore, [Majestic et al. \(2009b\)](#) suggested that
 434 anthropogenic aerosol Fe may explain the lower $\delta^{56}\text{Fe}$ for PM_{2.5} than PM₁₀.

435 [Mead et al. \(2013\)](#) collected coarse (PM_{>2.5}) and fine (PM_{2.5}) aerosol particles in Bermuda
 436 during 2011-2012. As shown in Figure 3, total Fe concentrations were similar for fine and
 437 coarse particles throughout the year, and elevated Fe concentrations in both size fractions were
 438 observed during the high dust season ([Mead et al., 2013](#)). For total Fe in coarse particles, $\delta^{56}\text{Fe}$
 439 values were similar to the UCC and exhibited no apparent seasonal variation, with an average
 440 value ($+0.10 \pm 0.06\text{‰}$, 1 σ); in contrast, for total Fe in fine particles, $\delta^{56}\text{Fe}$ values were
 441 significantly higher in the high dust season ($+0.08 \pm 0.05\text{‰}$, 1 σ) than the low dust season ($-$
 442 $0.10 \pm 0.14\text{‰}$, 1 σ), implying significant contribution of non-dust sources to aerosol Fe in fine
 443 particles during the low dust season ([Mead et al., 2013](#)). Furthermore, biomass burning was
 444 invoked to potentially explain the lighter Fe in fine particles ([Mead et al., 2013](#)) due to lower
 445 $\delta^{56}\text{Fe}$ reported for various plant matters ([Guelke and Von Blanckenburg, 2007](#)).



446

447 **Figure 3.** Concentrations (a) and $\delta^{56}\text{Fe}$ values (b) of total Fe in coarse and fine particles
 448 collected in Bermuda in 2011-2012. The shaded area represents the high dust season when the
 449 sampling site was impacted by Saharan dust aerosol. Reproduced with permission from Mead
 450 et al. (2013).

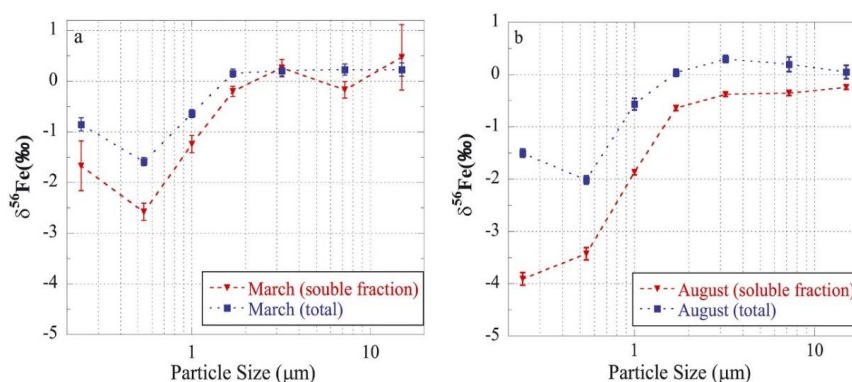
451

452 3.3.2 Studies published since 2016

453 For fine ($\text{PM}_{2.5}$) and coarse ($\text{PM}_{>2.5}$) ambient aerosol particles collected over the
 454 northwestern Pacific, Kurisu et al. (2016a) found that the $\delta^{56}\text{Fe}$ values of total Fe were
 455 significantly lower in fine particles ($-1.17 \pm 0.11\text{‰}$ and $-1.72 \pm 0.14\text{‰}$) when compared to coarse
 456 particles ($-0.11 \pm 0.14\text{‰}$ and $-0.32 \pm 0.23\text{‰}$). Kurisu et al. (2016a) also measured Fe isotopic
 457 compositions for size-fractionated aerosol samples collected at Hiroshima, Japan, and found
 458 $\delta^{56}\text{Fe}$ to be as low as -2.01‰ for total aerosol Fe and -3.91‰ for soluble aerosol Fe. Figure 4
 459 shows the particle size-dependence of $\delta^{56}\text{Fe}$ reported by Kurisu et al. (2016a) and highlights
 460 some important features: 1) $\delta^{56}\text{Fe}$ of total Fe increased with increasing particle size, and at >1.3
 461 μm were similar to desert dust; 2) at a given particle size, $\delta^{56}\text{Fe}$ were lower for soluble Fe than
 462 total Fe; 3) $\delta^{56}\text{Fe}$ were lower in August for both total and soluble Fe, when compared to March



463 (when the impact of Asian desert dust was larger). Furthermore, Fe solubility, which appeared
 464 to be higher in August than March, increased with a decrease in particle size for both months.
 465 Overall, the work by Kurisu et al. (2016a) suggested that anthropogenic Fe, which is more
 466 soluble and isotopically lighter than desert dust Fe, was relatively concentrated in finer particles.
 467 This conclusion was further supported by Fe speciation via X-ray absorption fine structure
 468 (XAFS) spectroscopy analysis (Kurisu et al., 2016a).



469
 470 **Figure 4.** Size-resolved $\delta^{56}\text{Fe}$ of total and soluble Fe for aerosol particles collected at
 471 Hiroshima (Japan) in March (a) and August (b). Reproduced with permission from Kurisu et
 472 al. (2016a).

473
 474 Kurisu and Takahashi (2019) measured isotopic compositions of aerosol Fe in ambient air
 475 masses affected by a biomass burning event in Tochigi, Japan. Before and after biomass
 476 burning, $\delta^{56}\text{Fe}$ was measured to be $+0.04 \pm 0.08$ ‰ on average for coarse particles ($>1 \mu\text{m}$), while
 477 much lower $\delta^{56}\text{Fe}$ values were found for fine particles ($<1 \mu\text{m}$). During the biomass burning
 478 event, $\delta^{56}\text{Fe}$ values of coarse particles were identical to those before and after the event;
 479 however, $\delta^{56}\text{Fe}$ values for fine particles, though still lower than those for coarse particles during



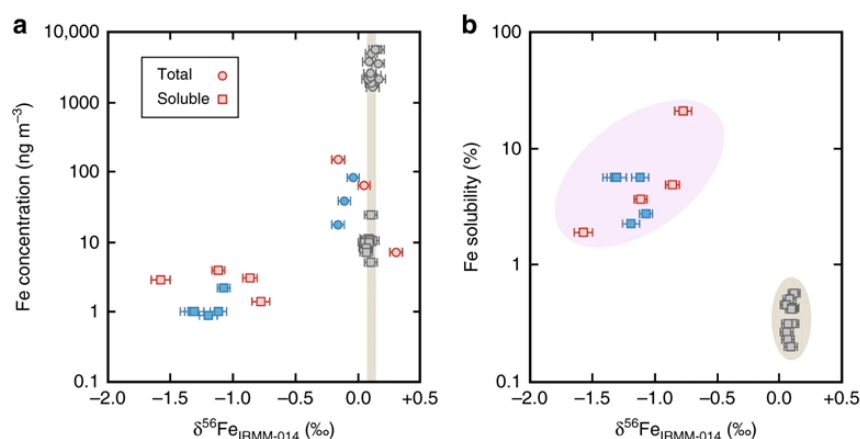
480 the biomass burning event, were found to be higher when compared to those for fine particles
481 before and after the event. As a result, [Kurusu and Takahashi \(2019\)](#) suggested that the low
482 $\delta^{56}\text{Fe}$ measured for fine particles before and after the biomass burning event was due to the
483 influence of anthropogenic combustion, and that Fe in biomass burning aerosols did not exhibit
484 low $\delta^{56}\text{Fe}$. [Kurusu and Takahashi \(2019\)](#) further speculated that combustion temperature during
485 the biomass burning event was not high enough to cause Fe isotopic fractionation (and thus
486 lead to lighter Fe in emitted aerosol particles). In addition, when compared to total Fe, soluble
487 Fe was found to have lower or similar $\delta^{56}\text{Fe}$ values ([Kurusu and Takahashi, 2019](#)).

488 Another study by [Kurusu et al. \(2019\)](#) examined Fe solubility and isotopic compositions
489 of size-resolved aerosol particles collected in Chiba, Japan, heavily impacted by steel plant
490 emissions, and found higher Fe solubility in fine particles ($<1.3\ \mu\text{m}$) than coarse particles (>1.3
491 μm). Moreover, $\delta^{56}\text{Fe}$ ranged from -0.42 to $+0.33\text{‰}$ for coarse particles, likely reflecting Fe
492 isotopic compositions in steel slags and raw materials; Fe in fine particles appeared to be
493 isotopically lighter ($\delta^{56}\text{Fe}$ in the range of -3.53 to -0.37‰), implying Fe fractionation during
494 evaporation under high temperature ([Kurusu et al., 2019](#)). [Kurusu et al. \(2019\)](#) also found that
495 soluble Fe (extracted using ultrapure water or simulated rainwater) was isotopically lighter than
496 total Fe.

497 [Conway et al. \(2019\)](#) measured solubility and isotopic compositions of aerosol Fe
498 collected over the North Atlantic during winter. Air masses originating from the Saharan region
499 were characterized by higher concentrations of aerosol Fe and lower Fe solubility, and average
500 $\delta^{56}\text{Fe}$ were reported to be $+0.12\pm0.03\text{‰}$ for total Fe and $+0.09\pm0.02\text{‰}$ for soluble Fe (Figure
501 5), similar to desert dust ([Conway et al., 2019](#)). In contrast, air masses originating from Europe



502 and North America exhibited lower concentrations of aerosol Fe but much higher Fe solubility,
 503 and compared to Saharan air masses, $\delta^{56}\text{Fe}$ in European and North American air masses were
 504 much lower for soluble Fe (mean: -0.91‰) but only slightly lower for total Fe
 505 (mean: $-0.12 \pm 0.06\text{‰}$). As a result, Conway et al. (2019) suggested that anthropogenic Fe with
 506 higher solubility but lower $\delta^{56}\text{Fe}$ made a large contribution to total Fe and especially soluble
 507 Fe in European and North American air masses. This work further utilized a two-component
 508 mixing model with assigned endmember $\delta^{56}\text{Fe}$ values for natural and anthropogenic Fe ($+0.09\text{‰}$
 509 and -1.60‰ , respectively) to constrain the sources of soluble Fe. Fossil fuel combustion
 510 comprised up to $\sim 50\text{--}100\%$ of soluble Fe for air masses originating from North America and
 511 Europe (Conway et al., 2019), while the Saharan air masses were characterized by $\sim 100\%$
 512 natural Fe from desert dust.



513
 514 **Figure 5.** Measured $\delta^{56}\text{Fe}$ of total and soluble Fe versus (a) Fe concentrations and (b) Fe
 515 solubility. Aerosol particles from different air masses are separated with colors (gray: Saharan
 516 air masses; red: European air masses; blue: North American air masses). Reproduced with
 517 permission from Conway et al. (2019).

518



519 [Kurusu et al. \(2021\)](#) investigated Fe solubility, speciation, and isotopic compositions of
520 fine ($<2.5\ \mu\text{m}$) and coarse ($>2.5\ \mu\text{m}$) particles collected over the northwestern Pacific, and the
521 air masses they sampled broadly came from East Asia, central/eastern Pacific, or from over the
522 northern Pacific. The average $\delta^{56}\text{Fe}$ value of total Fe was $+0.25\pm0.14\text{‰}$ and $+0.23\pm0.17\text{‰}$ for
523 coarse and fine particles in air masses from central/eastern Pacific, respectively, and
524 $+0.14\pm0.10\text{‰}$ and $+0.43\pm0.17\text{‰}$ from the North Pacific; from East Asia, average $\delta^{56}\text{Fe}$ of total
525 Fe was determined to be $-1.10\pm0.63\text{‰}$ for fine particles, much lower than that for coarse
526 particles ($-0.02\pm0.14\text{‰}$, close to desert dust). For air masses from East Asia, $\delta^{56}\text{Fe}$ values of
527 total Fe were found to be negatively correlated with Fe solubility ([Kurusu et al., 2021](#)),
528 suggesting that combustion Fe had lower $\delta^{56}\text{Fe}$ and higher solubility; the relative contribution
529 of combustion to total aerosol Fe could be up to 50% for fine particles and 6% for coarse
530 particles, estimated using obtained Fe isotopic data. For the three aerosol samples which
531 contained enough soluble Fe for isotopic analysis, $\delta^{56}\text{Fe}$ were significantly lower for soluble
532 Fe (as low as $-2.23\pm0.04\text{‰}$) than total Fe ([Kurusu et al., 2021](#)), indicating preferential
533 dissolution of Fe with lower $\delta^{56}\text{Fe}$ (for example, perhaps anthropogenic or combustion Fe).

534 [Zuo et al. \(2022\)](#) analyzed Fe isotopic compositions of magnetic materials in fine (<2.5
535 μm) and coarse particles ($>2.5\ \mu\text{m}$) collected in Beijing during March-May 2021 when dust
536 storms occurred. The average $\delta^{56}\text{Fe}$ was determined to be $+0.15\pm0.04\text{‰}$ in coarse particles
537 (similar to desert dust), indicating desert dust as the dominant source for magnetic Fe in coarse
538 particles. For fine particles, the average $\delta^{56}\text{Fe}$ was $-0.57\pm0.08\text{‰}$ during the non-dust-storm
539 period, suggesting important contribution from anthropogenic sources; it increased



540 to $-0.26 \pm 0.21\text{‰}$ during the dust-storm period, implying an enhanced contribution of desert dust
541 when compared to the non-dust-storm period.

542 A recent study (Kurusu et al., 2024) measured isotopic composition of total and soluble Fe
543 in TSP and size-resolved aerosol particles collected over the subarctic North Pacific. Overall,
544 for a given sample, $\delta^{56}\text{Fe}$ was similar or lower for soluble Fe, when compared to total Fe
545 (Kurusu et al., 2024): $\delta^{56}\text{Fe}$ ranged from -0.5 to $+0.4\text{‰}$ and from -1.87 to $+0.28\text{‰}$ for total and
546 soluble Fe in TSP, and from -2.8 to $+0.5\text{‰}$ for total Fe in the size-resolved aerosol samples. A
547 two-component mixing model was used to estimate the contribution of combustion to total and
548 soluble aerosol Fe, assuming that crustal and combustion Fe had endmembers values of $+0.1\text{‰}$
549 and -4.3‰ , respectively. The contribution of combustion could reach up to 13% for total Fe
550 and 45% for soluble Fe in TSP samples, and was highest in the coastal region of East Asia
551 (Kurusu et al., 2024).

552 Hsieh and Ho (2024) reported isotopic compositions of total and soluble (ultrapure water
553 leached) Fe for size-resolved aerosol particles collected on a small islet in the East China Sea.
554 The $\delta^{56}\text{Fe}$ values of total Fe ranged from -0.08 to $+0.16\text{‰}$ for large particles ($>1.6\text{ }\mu\text{m}$),
555 showing no dependence on particle size; however, they decreased to -1.16 to -0.06‰ and
556 further to -3.35 to -0.45‰ for particles in the size range of $1.0\text{-}1.6$ and $0.57\text{-}1.0\text{ }\mu\text{m}$,
557 respectively (Hsieh and Ho, 2024). Fe solubility was significantly correlated with $\delta^{56}\text{Fe}$ of total
558 Fe, suggesting significant contribution of anthropogenic sources to soluble Fe. In addition,
559 soluble Fe was isotopically lighter than total Fe, especially for fine particles ($0.57\text{-}1.0$ and 1.0-
560 $1.6\text{ }\mu\text{m}$). The contribution of anthropogenic sources was estimated to be 3.5-7.6% for total Fe



561 and 22-85% for soluble Fe (Hsieh and Ho, 2024), using a two-component mixing model which
 562 assumed $\delta^{56}\text{Fe}$ endmember values to be +0.1 and -4.4‰ for lithogenic and anthropogenic Fe.

563 Most recently, Bunnell et al. (2025) measured $\delta^{56}\text{Fe}$ of TSP as well as coarse ($>0.95\ \mu\text{m}$)
 564 and fine ($<0.95\ \mu\text{m}$) aerosols collected from the North Pacific GEOTRACES GP15 section
 565 (along 152°W , from 52°N to 20°S) during a low dust season (September-November 2018). In
 566 Asian Outflow deployments, total Fe in TSP and coarse particles had $\delta^{56}\text{Fe}$ values similar to
 567 the UCC, ranging from -0.03 and +0.07‰ and +0.02 to +0.20‰, respectively (Bunnell et al.,
 568 2025); however, total Fe in fine particles within the Asian Outflow was isotopically lighter
 569 (with $\delta^{56}\text{Fe}$ in the range of -0.39 to -0.25‰), indicative of the contribution of anthropogenic
 570 Fe. In the Equatorial Pacific, $\delta^{56}\text{Fe}$ of total Fe ranged from +0.15 to +0.41‰ for TSP, +0.15 to
 571 +0.27‰ for coarse particles, and +0.06 to +0.36‰ for fine particles (Bunnell et al., 2025),
 572 similar to or larger than the UCC. Heavier Fe observed in the Equatorial Pacific was attributed
 573 to wildfire soil Fe from western North America (Californian wildfires), based on the
 574 information that up to 64% of aerosol Fe produced in wildfire is derived from soil due to
 575 pyroconvective entrainment (Hamilton et al., 2022) and that $\delta^{56}\text{Fe}$ are in the range of +0.20 to
 576 +0.95‰ for Californian soils (Johnson et al., 2020). Although large differences in $\delta^{56}\text{Fe}$ of total
 577 Fe were observed between Asian Outflow and Equatorial Pacific aerosols, soluble aerosol Fe
 578 was generally light ($\delta^{56}\text{Fe}$ ranging from -1.28 to +0.02‰) throughout the transect (Bunnell et
 579 al., 2025), attributed to influence of anthropogenic Fe.

580 3.3.3 Discussion

581 Most field measurements found for total Fe in ambient aerosols, the $\delta^{56}\text{Fe}$ values were
 582 similar to or lower than UCC (Beard et al., 2003a; Waeles et al., 2007; Flament et al., 2008;



583 [Majestic et al., 2009b](#); [Mead et al., 2013](#); [Kurusu et al., 2016a](#); [Conway et al., 2019](#); [Kurusu et](#)
584 [al., 2019](#); [Kurusu and Takahashi, 2019](#); [Kurusu et al., 2021](#); [Zuo et al., 2022](#); [Kurusu et al., 2024](#)).
585 From these studies which reported lower $\delta^{56}\text{Fe}$ for total Fe in ambient aerosols ([Majestic et al.,](#)
586 [2009b](#); [Mead et al., 2013](#); [Kurusu et al., 2016a](#); [Conway et al., 2019](#); [Kurusu et al., 2019](#); [Kurusu](#)
587 [and Takahashi, 2019](#); [Kurusu et al., 2021](#); [Zuo et al., 2022](#)), two features can generally be
588 identified. First, when compared to those dominated by desert dust aerosol, $\delta^{56}\text{Fe}$ values for
589 total aerosol Fe were lower in air masses severely influenced by anthropogenic emissions
590 ([Majestic et al., 2009b](#); [Mead et al., 2013](#); [Kurusu et al., 2016a](#); [Conway et al., 2019](#); [Kurusu et](#)
591 [al., 2021](#); [Zuo et al., 2022](#)). Second, $\delta^{56}\text{Fe}$ values frequently appeared to be lower for smaller
592 particles than larger particles ([Majestic et al., 2009b](#); [Mead et al., 2013](#); [Kurusu et al., 2016a](#);
593 [Kurusu et al., 2019](#); [Kurusu and Takahashi, 2019](#); [Kurusu et al., 2021](#); [Zuo et al., 2022](#); [Hsieh](#)
594 [and Ho, 2024](#)).

595 Only a few studies ([Waeles et al., 2007](#); [Kurusu et al., 2016a](#); [Conway et al., 2019](#); [Kurusu](#)
596 [et al., 2019](#); [Kurusu and Takahashi, 2019](#); [Kurusu et al., 2021](#); [Bunnell et al., 2025](#)) reported
597 isotopic compositions of soluble Fe in ambient aerosols, and some of them ([Kurusu et al., 2016a](#);
598 [Conway et al., 2019](#); [Kurusu et al., 2019](#); [Kurusu and Takahashi, 2019](#); [Kurusu et al., 2021](#);
599 [Bunnell et al., 2025](#)) reported lower $\delta^{56}\text{Fe}$ for soluble aerosol Fe (relative to UCC). Similar to
600 total Fe, $\delta^{56}\text{Fe}$ of soluble Fe were found be lower in air masses with severe impacts by
601 anthropogenic emissions ([Kurusu et al., 2016a](#); [Conway et al., 2019](#)), when compared to air
602 masses dominated by desert dust; furthermore, $\delta^{56}\text{Fe}$ of soluble Fe decreased with decrease in
603 particle size ([Kurusu et al., 2016a](#); [Kurusu et al., 2019](#)). Compared to total aerosol Fe, soluble
604 aerosol Fe was found to be isotopically lighter ([Kurusu et al., 2016a](#); [Conway et al., 2019](#);



605 [Kurusu et al., 2019](#); [Kurusu et al., 2021](#)), especially for smaller particles in air masses severely
606 affected by anthropogenic emissions.

607 The overall features of isotopic compositions of total and soluble Fe in ambient aerosols,
608 revealed by a limited number of field studies, can be possibly explained by anthropogenic Fe
609 (such as fossil fuel combustion, industrial emission, and etc.) which is isotopically lighter, more
610 soluble, and enriched in fine particles, when compared to desert dust Fe. This explanation is
611 elaborated upon below. First, as anthropogenic Fe is isotopically lighter than desert dust Fe,
612 lower $\delta^{56}\text{Fe}$ are expected in air masses severely affected by anthropogenic emissions, when
613 compared to air masses dominated by desert dust. Second, since in general anthropogenic Fe
614 is enriched in fine particles while desert dust Fe is enriched in coarse particles, we expect Fe
615 in fine particles to be isotopically lighter than coarse particles. Lastly, anthropogenic Fe is more
616 soluble than desert dust Fe, and therefore the net $\delta^{56}\text{Fe}$ values are lower for overall soluble Fe
617 than total Fe.

618 Some studies ([Majestic et al., 2009b](#); [Kurusu et al., 2016a](#); [Conway et al., 2019](#); [Kurusu et](#)
619 [al., 2019](#); [Kurusu et al., 2021](#); [Zuo et al., 2022](#)) have suggested that isotopically lighter $\delta^{56}\text{Fe}$ in
620 ambient aerosols can be explained by anthropogenic emission (such as fossil fuel combustion
621 and metal smelting). [Mead et al. \(2013\)](#) suggested biomass burning as the likely source of
622 isotopically lighter Fe in ambient aerosols, while more recent studies ([Conway et al., 2019](#);
623 [Kurusu and Takahashi, 2019](#)) did not lend support to this idea. Furthermore, several studies
624 ([Labatut et al., 2014](#); [Conway et al., 2019](#); [Kurusu et al., 2021](#); [Kurusu et al., 2024](#); [Bunnell et](#)
625 [al., 2025](#)) observed significantly higher $\delta^{56}\text{Fe}$ (than UCC) for ambient aerosol Fe. This
626 observation has been variably attributed to coal and oil fly ash ([Mead et al., 2013](#); [Kurusu et al.,](#)



2016b; Li et al., 2022), or most recently to wildfire emissions (Bunnell et al., 2025). Further work to investigate the source signatures of different emissions is required (as discussed in Section 3.2).

3.4 Modeling studies of isotopic compositions of ambient aerosol Fe

Conway et al. (2019) compared measured solubility and isotopic compositions of aerosol Fe over the Atlantic with those predicted using a 3-D model (Community Atmosphere Model v4, CAM4), in which $\delta^{56}\text{Fe}$ endmember values were set to +0.09‰ for desert dust and -1.6‰ for anthropogenic aerosol, as constrained by their observation. Compared to measurements, although the default CAM4 model could reasonably well reproduce Fe solubility for European and North American aerosols, it overestimated Fe solubility for Saharan aerosols; furthermore, it failed to simulate $\delta^{56}\text{Fe}$ for soluble aerosol Fe (Conway et al., 2019). The model could much better reproduce measured Fe solubility and $\delta^{56}\text{Fe}$ only if Fe solubility of dust aerosol was reduced from 25% to 10% and anthropogenic Fe aerosol emission was increased by a factor of 5. Therefore, Conway et al. (2019) suggested that the contribution of anthropogenic emission to soluble aerosol Fe might have been significantly underestimated.

Kurisu et al. (2021) employed a 3-D model (IMPACT) to simulate isotopic compositions of total Fe in fine ($<2.5\ \mu\text{m}$) and coarse ($>2.5\ \mu\text{m}$) particles over the northwestern Pacific, and in their simulation $\delta^{56}\text{Fe}$ were set to 0‰ for desert dust and -4.7‰ to -3.9‰ for combustion aerosol. The modelled $\delta^{56}\text{Fe}$ agreed well with observations for fine particles but were significantly lower for coarse particles. This underestimation may result from using the same endmember $\delta^{56}\text{Fe}$ values for fine and coarse particles in the model (Kurisu et al., 2021); in other words, if the endmember $\delta^{56}\text{Fe}$ value of combustion Fe was set to be larger for coarse



649 particles than fine particles, the model may reproduce the observed $\delta^{56}\text{Fe}$ for both fine and
650 coarse particles.

651 A very recent study (Bunnell et al., 2025) compared their measured total Fe concentrations
652 and isotopic compositions for aerosols collected from the North Pacific GEOTRACES GP15
653 section with those simulated by Community Atmosphere Model v6 (CAM6). Based on
654 previous work by Conway et al. (2019), using the initial endmember values (+0.1‰ for dust,
655 and -1.60‰ for anthropogenic, wildfire and shipping aerosols) in the model caused large
656 underestimations in $\delta^{56}\text{Fe}$ (Bunnell et al., 2025). When compared to the initial values, the
657 optimal endmember values (which led to best agreement between measured and simulated
658 $\delta^{56}\text{Fe}$ of ambient total aerosol Fe) remained unchanged for dust and anthropogenic aerosol, but
659 increased to +0.8‰ and +0.5‰ for wildfire and shipping, respectively (Bunnell et al., 2025).

660 Overall, modeling studies which simulate isotopic compositions of ambient aerosol Fe are
661 very limited at present. As measurements of isotopic compositions of ambient aerosol Fe and
662 aerosol Fe emitted from various sources are increasing, it is expected that more modeling
663 studies will include isotopic compositions to better constrain sources of aerosol Fe.

664 3.5 Fe isotopic fractionation induced by chemical processing

665 Chemical processes which change the speciation of Fe in the environment may also lead
666 to isotopic fractionation that may attenuate or drive isotopic signatures observed in ambient
667 aerosols. As summarized in Table 1, in this section we discuss previous studies which
668 investigated Fe isotopic fractionation induced by a few types of reactions of potential relevance
669 for atmospheric aerosol Fe, namely proton-promoted dissolution, redox reaction, reductive
670 dissolution, ligand complexation and ligand-promoted dissolution. We refer the readers to Yin



et al. (2023) for a more comprehensive discussion of Fe isotopic fractionation induced by biogeochemical processes.

673

Table 1. Fe isotopic fractionation caused by chemical processes relevant for atmospheric aerosol Fe. In this table, pFe(II) represents particulate Fe, dFe(III) and dFe(II) represent dissolved Fe(III) and Fe(II), and dFe(III)-ligand represent dissolved Fe(III) complexed with ligands.

chemical process	chemical formula	$\Delta^{56}\text{Fe}$	Ref.
proton-promoted dissolution	pFe(III) \rightarrow dFe(III)	-1.8‰ to +0‰	a
redox reaction	dFe(III) \rightarrow dFe(II)	-2.8‰	b
reductive dissolution	pFe(III) \rightarrow dFe(II)	-2.2‰ to -1‰	c
ligand complexation	dFe(III) + ligand \rightarrow dFe(III)-ligand	+0.3‰ to +0.6‰	d
ligand-promoted dissolution	pFe(III) + ligand \rightarrow dFe(III)-ligand	-1.3‰ to +0‰	e

a: Skulan et al. (2002), Wiederhold et al. (2006), Chapman et al. (2009), Kiczka et al. (2010);

b: Johnson et al. (2002), Welch et al. (2003);

c: Wiederhold et al. (2006);

d: Wiederhold et al. (2006), Dideriksen et al. (2008);

e: Brantley et al. (2001), Wiederhold et al. (2006), Chapman et al. (2009), Kiczka et al. (2010).

683

3.5.1 Proton-promoted dissolution

Wiederhold et al. (2006) examined goethite dissolution in 0.5 mol/L HCl and found that the isotopic composition for dissolved Fe in the solution was not statistically different from that of original goethite over the entire experiment (up to 315 days), suggesting that goethite dissolution in HCl solution did not lead to Fe isotopic fractionation. However, some other



689 studies (Skulan et al., 2002; Chapman et al., 2009; Kiczka et al., 2010) suggest that proton-
690 promoted dissolution could lead to significant Fe isotopic fractionation. For example, in the
691 early stage of hematite dissolution in 0.9 mol/L HCl, dissolved Fe was much isotopically lighter
692 due to kinetic isotopic fractionation and $\Delta^{56}\text{Fe}$ reached $-1.32 \pm 0.12\text{‰}$ (Skulan et al., 2002);
693 however, the effect of kinetic isotopic fractionation became smaller with time and eventually
694 isotopic compositions were identical between dissolved Fe and hematite. Significant Fe
695 isotopic fractionation, with $\Delta^{56}\text{Fe}$ being as low as -1.8‰ , was reported for dissolution of granite
696 and basalt in 0.5 mol/L HCl (Chapman et al., 2009). Dissolution of biotite and chlorite in HCl
697 solution (pH = 4) also led to significant Fe isotopic fractionation (Kiczka et al., 2010), and
698 $\Delta^{56}\text{Fe}$ reached as low as -1.4‰ ; furthermore, Kiczka et al. (2010) found the presence of K^+ in
699 the solution would facilitate isotopic fractionation.

700 It remains unclear why previous studies (Skulan et al., 2002; Wiederhold et al., 2006;
701 Chapman et al., 2009; Kiczka et al., 2010) reported different Fe isotopic fractionation effects
702 induced by proton-promoted dissolution, and difference in Fe mineralogy (thus bonding
703 strength) may play a role.

704 3.5.2 Redox reaction and reductive dissolution

705 Johnson et al. (2002) investigated Fe isotopic fractionation for aqueous redox of Fe(III)
706 to Fe(II) at room temperature, and observed similar degrees of Fe isotopic fractionation at pH
707 of 2 and 3: Fe(II) was isotopically lighter than Fe(III), and $\Delta^{56}\text{Fe}$ was determined to
708 be $-2.75 \pm 0.15\text{‰}$ when the reaction reached equilibrium. Welch et al. (2003) examined the
709 effects of temperatures (0 and 22 °C) and Cl^- concentrations on Fe isotopic fractionation in
710 aqueous redox of Fe(III) to Fe(II) and observed significant enrichment of isotopically lighter



711 Fe in Fe(II). The average $\Delta^{56}\text{Fe}$ values were $-2.76 \pm 0.09\text{‰}$, $-2.87 \pm 0.22\text{‰}$, and $-2.76 \pm 0.06\text{‰}$ at
712 22 °C when Cl^- concentrations in the solution were 0, 11, and 111 mmol/L (Welch et al., 2003),
713 respectively, suggesting no significant impact of Cl^- ; moreover, a decrease in temperature from
714 22 to 0 °C resulted in larger Fe isotopic fractionation, and the average $\Delta^{56}\text{Fe}$ was $-3.25 \pm 0.38\text{‰}$
715 at 0 °C in the absence of Cl^- in the aqueous solutions. The two previous studies (Johnson et al.,
716 2002; Welch et al., 2003) both suggested that isotopic fractionation occurred when Fe(III) was
717 reduced to Fe(II) in the solution, with Fe(II) being isotopically lighter than Fe(III).

718 Wiederhold et al. (2006) explored reductive dissolution of goethite in 0.5 mmol/L oxalate
719 solution irradiated using a solar simulator. The dissolved fraction was isotopically lighter in the
720 initial stage, with $\Delta^{56}\text{Fe}$ being as low as -1.6‰ (Wiederhold et al., 2006); this effect gradually
721 became smaller and the isotopic composition of dissolved Fe eventually was identical to bulk
722 goethite.

723 3.5.3 Ligand complexation and ligand-promoted dissolution

724 Wiederhold et al. (2006) showed that at equilibrium Fe isotopic composition was heavier
725 for the Fe(III)-oxalate complex than free Fe(III) in the solution ($\Delta^{56}\text{Fe} = +0.3\text{‰}$). Another study
726 (Dideriksen et al., 2008) found that the formation of the Fe(III)-desferrioxamine B complex in
727 the solution caused Fe isotopic fractionation, and $\Delta^{56}\text{Fe}$ was determined to be $+0.6\text{‰}$ at
728 equilibrium. These experimental results (Wiederhold et al., 2006; Dideriksen et al., 2008) are
729 consistent with theoretical work which predicted enrichment of heavier isotopes in stronger
730 bonding environments under equilibrium fractionation (Schauble, 2004; Dideriksen et al., 2008;
731 Ilina et al., 2013).



732 [Brantley et al. \(2001\)](#) investigated ligand-promoted dissolution of hornblende in oxalate
733 (0.024 mmol/L, pH = 7), and found that dissolved Fe was isotopically lighter than that in bulk
734 hornblende ($\Delta^{56}\text{Fe} = -0.3\text{‰}$). In the early stage of ligand-promoted dissolution of goethite in
735 oxalate (5 mmol/L, pH = 3), significant Fe isotopic fractionation was observed and $\Delta^{56}\text{Fe}$ could
736 reach as low as -1.2‰ ([Wiederhold et al., 2006](#)); after that, $\delta^{56}\text{Fe}$ of dissolved Fe increased
737 gradually with reaction time, and eventually was even slightly larger than bulk goethite due to
738 equilibrium isotope effects. Significant Fe isotopic fractionation occurred during ligand-
739 promoted dissolution (5 mmol/L oxalate) of granite and basalt at room temperature ([Chapman](#)
740 [et al., 2009](#)), and $\Delta^{56}\text{Fe}$ was down to -1.3‰ ; similarly, [Kiczka et al. \(2010\)](#) found that ligand-
741 promoted dissolution (5 mmol/L oxalate) of biotite and chlorite resulted in Fe isotopic
742 fractionation ($\Delta^{56}\text{Fe}$ as low as -0.5‰). In summary, ligand-promoted dissolution resulted in
743 significant Fe isotopic fractionation, and the dissolved Fe appeared to be isotopically lighter
744 due to kinetic fractionation effects.

745 **3.5.4 Discussion**

746 Previous studies, as summarized in Table 1, provide important insights into Fe isotopic
747 fractionation induced by chemical processes which may also occur in the atmosphere. However,
748 experimental conditions used in these studies, including minerals examined, may not be of
749 direct relevance for atmospheric aerosols. Recently, some work started to explore the effects of
750 atmospheric chemical processing on Fe isotopic fractionation, as showcased below.

751 [Mulholland et al. \(2021\)](#) studied Fe isotope fractionation during dissolution of Fe-Mn
752 alloy metallurgy fly ash in synthetic cloud water (pH = 2) under UV/VIS radiation from a solar
753 simulator. Compared to Fe in fly ash, dissolved Fe was isotopically lighter in the first stage of



dissolution (0-60 min) due to kinetic isotopic effects, with $\Delta^{56}\text{Fe}$ as low as $-0.28 \pm 0.10\%$ (Mulholland et al., 2021); in the second stage of dissolution (60-120 min), dissolved Fe was isotopically heavier due to equilibrium isotopic effects, with $\Delta^{56}\text{Fe}$ as high as $+0.23 \pm 0.09\%$ (Mulholland et al., 2021). A following study (Maters et al., 2022) further investigated Fe isotope fractionation during the initial stage (0-60 min) of dissolution of Tunisian desert dust and Fe-Mn alloy metallurgy fly ash; compared to Mulholland et al. (2021), the synthetic cloud water used by Maters et al. (2022) additionally contained 1 mmol/L oxalate. Compared to Fe in original particles, dissolved Fe was isotopically lighter for both desert dust and fly ash (Maters et al., 2022), and the extent of Fe isotopic fractionation during dissolution appeared to be larger for desert dust.

4. Perspectives

In the last 10-20 years Fe isotopic analysis has been increasingly used in aerosol research (as discussed in Section 3), and has been demonstrated to be a promising way to differentiate sources of total and soluble aerosol Fe, and to quantify the relative importance of different sources. Several future research directions are proposed here to further enhance the usefulness of Fe isotopes in atmospheric aerosol research.

(1) The precision of $\delta^{56}\text{Fe}$ measurements via MC-ICP-MS can reach ± 0.02 to $\pm 0.06\%$ (2σ) at present, and this should be enough for most applications in atmospheric aerosols. The optimal mass of Fe required for isotopic analysis is around 20-100 ng. It is usually not difficult to collect enough total aerosol Fe for isotopic analysis with acceptable uncertainties, but can be challenging to collect enough soluble aerosol Fe. Therefore, further improvement in



775 analytical methods to reduce the minimum mass of Fe required is warranted to increase the
776 application of Fe isotopic analysis in aerosol research.

777 (2) Using Fe isotopes to constrain the sources of atmospheric aerosol Fe requires
778 constraints on isotopic signatures ($\delta^{56}\text{Fe}$ endmember values) of aerosol Fe from different
779 sources. The $\delta^{56}\text{Fe}$ endmember values are reasonably well understood for desert dust Fe, being
780 rather homogeneous and similar to UCC. However, so far only a limited number of studies
781 have measured $\delta^{56}\text{Fe}$ endmember values of non-desert-dust Fe (Table S1), and the number of
782 samples covered by each of these studies is typically small. The $\delta^{56}\text{Fe}$ endmember values have
783 large uncertainties for aerosol Fe from various non-desert-dust sources. Therefore, relevant
784 experimental measurements are highly needed to reduce these uncertainties.

785 (3) Up to now only a small number of studies (<20, as summarized in Table 2) have
786 measured isotopic compositions of ambient aerosol Fe, and the isotopic compositions were less
787 measured for soluble aerosol Fe than total aerosol Fe. Further application of Fe isotopes in
788 ambient aerosol research is encouraged, especially in HNLC regions where aerosol Fe
789 deposition may have large impacts on marine primary productivity and in regions where
790 anthropogenic and wildfire emission may have substantial contribution to total and soluble
791 aerosol Fe. Furthermore, additional insights can be gained via comparing source apportionment
792 results constrained using Fe isotopes with those obtained using correlation (Chuang et al., 2005;
793 Sholkovitz et al., 2009; Zhang et al., 2023) and factor analysis (Zhu et al., 2020; Chen et al.,
794 2024; Zhang et al., 2024).

795 (4) At present, isotopic compositions are assumed to be identical for total and soluble
796 aerosol Fe from a given source when Fe isotopes are used to constrain the sources of ambient



797 aerosol Fe. This assumption is yet to be verified as some laboratory studies indicate that
798 chemical processing in the atmosphere may lead to Fe isotopic fractionation (Section 3.5). As
799 a result, further studies should be carried out to understand isotopic fractionation of aerosol Fe
800 caused by chemical processing under atmospherically relevant conditions.

801 (5) We also encourage modeling studies to include isotopic compositions of aerosol Fe.
802 Comparison of modelled isotopic compositions of total and soluble aerosol Fe with
803 measurements (the number of which is increasing) can provide additional constraints to their
804 sources, in addition to using spatial and temporal variability of their concentrations.

805 (6) Particle size distribution and mineralogy play a critical role in deposition of soluble
806 aerosol Fe, because particle size largely dictates sources, chemical processing and fractional
807 solubility of aerosol Fe (Zhang et al., 2022; Chen et al., 2024) as well as its lifetime, transport
808 and deposition (Liu et al., 2024). A few studies (Mead et al., 2013; Kurisu et al., 2016a; Kurisu
809 et al., 2019; Kurisu and Takahashi, 2019; Kurisu et al., 2021; Kurisu et al., 2024) suggest that
810 isotopic compositions of total and soluble aerosol Fe change significantly with particle size,
811 implying variation of their sources with particle size. As a result, size-dependence of isotopic
812 compositions of total and soluble Fe deserves further investigation.

813 (7) Modeling work (Myriokefalitakis et al., 2015; Hamilton et al., 2020b; Hamilton et al.,
814 2020a; Bergas-Massó et al., 2023) suggests that when compared to the preindustrial era, the
815 relative contribution of desert dust, anthropogenic emission and biomass burning to total and
816 soluble aerosol Fe may have changed immensely. Measurements of isotopic compositions of
817 total and dissolved Fe in ice core samples (Conway et al., 2015; Xiao et al., 2020) can provide
818 valuable data to verify historical changes given by modeling simulations.



819

820 **Data availability.**

821 Data used in this review paper all come from previous studies.

822 **Author contribution.**

823 **Yifan Zhang:** formal analysis, writing – original draft, writing – review & editing;

824 **Rui Li:** formal analysis, writing – original draft, writing – review & editing;

825 **Zachary B. Bunnell:** writing – original draft, writing – review & editing;

826 **Yizhu Chen:** writing – original draft, writing – review & editing;

827 **Guanhong Zhu:** writing – review & editing;

828 **Jinlong Ma:** writing – review & editing;

829 **Guohua Zhang:** writing – review & editing;

830 **Tim M. Conway:** conceptualization, writing – original draft, writing – review & editing;

831 **Mingjin Tang:** conceptualization, formal analysis, writing – original draft, writing –
832 review & editing.

833 **Competing interests.**

834 The authors declare that they have no conflict of interest.

835 **Financial support.**

836 This work was sponsored by National Natural Science Foundation of China (42321003
837 and 42277088), Guangzhou Bureau of Science and Technology (2024A04J6533), Guangdong
838 Foundation for Program of Science and Technology Research (2023B1212060049), and
839 Scientific Committee on Oceanic Research (SCOR) Working Group 167 (Reducing



840 Uncertainty in Soluble aerosol Trace Element Deposition, RUSTED). Zachary B. Bunnell and

841 Tim M. Conway were supported by NSF Award OCE-1737136.

842

843



References:

- Baker, A. R. and Jickells, T. D.: Mineral particle size as a control on aerosol iron solubility, *Geophys. Res. Lett.*, 33, L17608, doi: 17610.11029/12006GL026557, 2006.
- Baker, A. R., Kanakidou, M., Nenes, A., Myriokefalitakis, S., Croot, P. L., Duce, R. A., Gao, Y., Guieu, C., Ito, A., Jickells, T. D., Mahowald, N. M., Middelburg, R., Perron, M. M. G., Sarin, M. M., Shelley, R., and Turner, D. R.: Changing atmospheric acidity as a modulator of nutrient deposition and ocean biogeochemistry, *Science Advances*, 7, eabd8800, 10.1126/sciadv.abd8800, 2021.
- Beard, B. L. and Johnson, C. M.: High precision iron isotope measurements of terrestrial and lunar materials, *Geochim. Cosmochim. Acta*, 63, 1653-1660, 1999.
- Beard, B. L. and Johnson, C. M.: Fe isotope variations in the modern and ancient earth and other planetary bodies, in: *Geochemistry of Non-Traditional Stable Isotopes*, edited by: Johnson, C. M., Beard, B. L., and Albarède, F., *Reviews in Mineralogy & Geochemistry*, 319-357, 2004.
- Beard, B. L., Johnson, C. M., Von Damm, K. L., and Poulson, R. L.: Iron isotope constraints on Fe cycling and mass balance in oxygenated Earth oceans, *Geology*, 31, 629-632, 2003a.
- Beard, B. L., Johnson, C. M., Skulan, J. L., Nealson, K. H., Cox, L., and Sun, H.: Application of Fe isotopes to tracing the geochemical and biological cycling of Fe, *Chemical Geology*, 195, 87-117, 2003b.
- Bergas-Massó, E., Gonçalves Ageitos, M., Myriokefalitakis, S., Miller, R. L., van Noije, T., Le Sager, P., Montané Pinto, G., and Pérez García-Pando, C.: Pre-Industrial, Present and Future Atmospheric Soluble Iron Deposition and the Role of Aerosol Acidity and Oxalate Under CMIP6 Emissions, *Earth's Future*, 11, e2022EF003353, <https://doi.org/10.1029/2022EF003353>, 2023.
- Boyd, P. W. and Ellwood, M. J.: The biogeochemical cycle of iron in the ocean, *Nature Geosci.*, 3, 675-682, 2010.
- Brantley, S. L., Liermann, L., and Bullen, T. D.: Fractionation of Fe isotopes by soil microbes and organic acids, *Geology*, 29, 535-538, 2001.
- Buck, C. S., Landing, W. M., and Resing, J. A.: Particle size and aerosol iron solubility: A high-resolution analysis of Atlantic aerosols, *Mar. Chem.*, 120, 14-24, 2010.
- Bunnell, Z. B., Sieber, M., Hamilton, D. S., Marsay, C. M., Buck, C. S., Landing, W. M., John, S. G., and Conway, T. M.: The influence of natural, anthropogenic, and wildfire sources on iron and zinc aerosols delivered to the North Pacific Ocean, *Geophys. Res. Lett.*, 52, e2024GL113877, <https://doi.org/10.1029/2024GL113877>, 2025.
- Chapman, J. B., Weiss, D. J., Shan, Y., and Lemburger, M.: Iron isotope fractionation during leaching of granite and basalt by hydrochloric and oxalic acids, *Geochim. Cosmochim. Acta*, 73, 1312-1324, 2009.
- Chen, T., Li, W., Guo, B., Liu, R., Li, G., Zhao, L., and Ji, J.: Reactive iron isotope signatures of the East Asian dust particles: Implications for iron cycling in the deep North Pacific, *Chem. Geol.*, 531, 119342, <https://doi.org/10.1016/j.chemgeo.2019.119342>, 2020.
- Chen, Y. Z., Wang, Z. Y., Fang, Z. Y., Huang, C. P., Xu, H., Zhang, H. H., Zhang, T. Y., Wang, F., Luo, L., Shi, G. L., Wang, X. M., and Tang, M. J.: Dominant Contribution of Non-dust Primary Emissions and Secondary Processes to Dissolved Aerosol Iron, *Environ. Sci. Technol.*, 58, 17355-17363, 2024.
- Chester, R., Murphy, K. J. T., Lin, F. J., Berry, A. S., Bradshaw, G. A., and Corcoran, P. A.: Factors controlling the solubilities of trace metals from non-remote aerosols deposited to the sea surface by the 'dry' deposition mode, *Mar. Chem.*, 42, 107-126, 1993.
- Chuang, P. Y., Duvall, R. M., Shafer, M. M., and Schauer, J. J.: The origin of water soluble particulate iron in the Asian atmospheric outflow, *Geophys. Res. Lett.*, 32, L07813, doi: 07810.01029/02004GL021946, 2005.
- Conway, T. M. and John, S. G.: Quantification of dissolved iron sources to the North Atlantic Ocean, *Nature*, 511, 212-215, 2014.
- Conway, T. M., Middelburg, R., and Schlitzer, R.: GEOTRACES: IRONING OUT THE DETAILS OF THE OCEANIC IRON SOURCES?, *Oceanography*, 37, 35-45, 2024.
- Conway, T. M., Horner, T. J., Plancherel, Y., and González, A. G.: A decade of progress in understanding cycles of trace elements and their isotopes in the oceans, *Chem. Geol.*, 580, 120381, 2021.
- Conway, T. M., Rosenberg, A. D., Adkins, J. F., and John, S. G.: A new method for precise determination of iron, zinc and cadmium stable isotope ratios in seawater by double-spike mass spectrometry, *Anal. Chim. Acta*, 793, 44-52, 2013.
- Conway, T. M., Wolff, E. W., Rothlisberger, R., Mulvaney, R., and Elderfield, H. E.: Constraints on soluble aerosol iron flux to the Southern Ocean at the Last Glacial Maximum, *Nature Communications*, 6, 10.1038/ncomms8850, 2015.
- Conway, T. M., Hamilton, D. S., Shelley, R. U., Aguilar-Islas, A. M., Landing, W. M., Mahowald, N. M., and John, S. G.: Tracing and constraining anthropogenic aerosol iron fluxes to the North Atlantic Ocean using iron isotopes, *Nature Comm.*, 10, 2628, 2019.
- Dauphas, N. and Rouxel, O.: Mass spectrometry and natural variations of iron isotopes, *Mass Spectrom. Rev.*, 25, 515-550, 2006.



- de Jong, J., Schoemann, V., Tison, J.-L., Becquevort, S., Masson, F., Lannuzel, D., Petit, J., Chou, L., Weis, D.,
and Mattielli, N.: Precise measurement of Fe isotopes in marine samples by multi-collector inductively
coupled plasma mass spectrometry (MC-ICP-MS), *Anal. Chim. Acta*, 589, 105-119, 2007.
- Desboeufs, K., Bon Nguyen, E., Chevaillier, S., Triquet, S., and Dulac, F.: Fluxes and sources of nutrient and trace
metal atmospheric deposition in the northwestern Mediterranean, *Atmos. Chem. Phys.*, 18, 14477-14492,
2018.
- Desboeufs, K. V., Sofikitis, A., Losno, R., Colin, J. L., and Ausset, P.: Dissolution and solubility of trace metals
from natural and anthropogenic aerosol particulate matter, *Chemosphere*, 58, 195-203, 2005.
- Dideriksen, K., Baker, J. A., and Stipp, S. L. S.: Kinetic and equilibrium Fe isotope fractionation between aqueous
Fe(III) and hematite, *Earth and Planetary Science Letters*, 269, 280-290, 2008.
- Fitzsimmons, J. N. and Conway, T. M.: Novel Insights into Marine Iron Biogeochemistry from Iron Isotopes,
Annu. Rev. Mar. Sci., 15, 383-406, 2023.
- Flament, P., Mattielli, N., Aimoz, L., Choël, M., Deboudt, K., Jong, J. d., Rimetz-Planchon, J., and Weis, D.: Iron
isotopic fractionation in industrial emissions and urban aerosols, *Chemosphere*, 73, 1793-1798, 2008.
- Gong, Y., Xia, Y., Huang, F., and Yu, H.: Average iron isotopic compositions of the upper continental crust:
constrained by loess from the Chinese Loess Plateau, *Acta Geochim.*, 36, 125-131, 2017.
- Guelke-Stelling, M. and von Blanckenburg, F.: Fe isotope fractionation caused by translocation of iron during
growth of bean and oat as models of strategy I and II plants, *Plant and Soil*, 352, 217-231, 2012.
- Guelke, M. and von Blanckenburg, F.: Fractionation of Stable Iron Isotopes in Higher Plants, *Environ. Sci.*
Technol., 41, 1896-1901, 2007.
- Hamilton, D. S., Scanza, R. A., Rathod, S. D., Bond, T. C., Kok, J. F., Li, L., Matsui, H., and Mahowald, N. M.:
Recent (1980 to 2015) Trends and Variability in Daily-to-Interannual Soluble Iron Deposition from Dust, Fire,
and Anthropogenic Sources, *Geophys. Res. Lett.*, 47, e2020GL089688, 2020a.
- Hamilton, D. S., Moore, J. K., Arneth, A., Bond, T. C., Carslaw, K. S., Hantson, S., Ito, A., Kaplan, J. O., Lindsay,
K., Nieradzik, L., Rathod, S. D., Scanza, R. A., and Mahowald, N. M.: Impact of Changes to the Atmospheric
Soluble Iron Deposition Flux on Ocean Biogeochemical Cycles in the Anthropocene, *Glob. Biogeochem.*
Cycle, 34, 10.1029/2019gb006448, 2020b.
- Hamilton, D. S., Perron, M. G. G., Bond, T. C., Bowie, A. R., Buchholz, R. R., Guieu, C., Ito, A., Maenhaut, W.,
Myriokefalitakis, S., Olgun, N., Rathod, S. D., Schepanski, K., Tagliabue, A., Wagner, R., and Mahowald, N.
M.: Earth, Wind, Fire, and Pollution: Aerosol Nutrient Sources and Impacts on Ocean Biogeochemistry, *Ann.*
Rev. Mar. Sci., 14, 303-330, 2022.
- Hsieh, C.-C. and Ho, T.-Y.: Contribution of Anthropogenic and Lithogenic Aerosol Fe in the East China Sea,
Journal of Geophysical Research: Oceans, 129, e2024JC021113, <https://doi.org/10.1029/2024JC021113>, 2024.
- Irina, S. M., Poitrasson, F., Lapitskiy, S. A., Alekhin, Y. V., Viers, J., and Pokrovsky, O. S.: Extreme iron isotope
fractionation between colloids and particles of boreal and temperate organic-rich waters, *Geochim.*
Cosmochim. Acta, 101, 96-111, 2013.
- Ito, A., Ye, Y., Baldo, C., and Shi, Z. B.: Ocean fertilization by pyrogenic aerosol iron, *NPJ Clim. Atmos. Sci.*, 4,
30, doi: 10.1038/s41612-41021-00185-41618, 2021.
- Ito, A., Myriokefalitakis, S., Kanakidou, M., Mahowald, N. M., Scanza, R. A., Hamilton, D. S., Baker, A. R.,
Jickells, T., Sarin, M., Bikkina, S., Gao, Y., Shelley, R. U., Buck, C. S., Landing, W. M., Bowie, A. R., Perron,
M. M. G., Guieu, C., Meskhidze, N., Johnson, M. S., Feng, Y., Kok, J. F., Nenes, A., and Duce, R. A.:
Pyrogenic iron: The missing link to high iron solubility in aerosols, *Science Adv.*, 5, eaau7671, doi:
7610.1126/sciadv.aau7671, 2019.
- Jickells, T. D., An, Z. S., Andersen, K. K., Baker, A. R., Bergametti, G., Brooks, N., Cao, J. J., Boyd, P. W., Duce,
R. A., Hunter, K. A., Kawahata, H., Kubilay, N., laRoche, J., Liss, P. S., Mahowald, N., Prospero, J. M.,
Ridgwell, A. J., Tegen, I., and Torres, R.: Global Iron Connections between Desert Dust, Ocean
Biogeochemistry, and Climate, *Science*, 308, 67-71, 2005.
- John, S. G. and Adkins, J.: The vertical distribution of iron stable isotopes in the North Atlantic near Bermuda,
Glob. Biogeochem. Cycle, 26, GB2034, DOI: 10.1029/2011GB004043, 2012.
- John, S. G. and Adkins, J. F.: Analysis of dissolved iron isotopes in seawater, *Marine Chemistry*, 119, 65-76, 2010.
- Johnson, C., Beard, B., and Weyer, S.: *Iron Geochemistry: An Isotopic Perspective*, Springer Cham,
Switzerland 2020.
- Johnson, C. M., Beard, B. L., Beukes, N. J., Klein, C., and O'Leary, J. M.: Ancient geochemical cycling in the
Earth as inferred from Fe isotope studies of banded iron formations from the Transvaal Craton, *Contributions*
to Mineralogy and Petrology, 144, 523-547, 2003.
- Johnson, C. M., Skulan, J. L., Beard, B. L., Sun, H., Neilson, K. H., and Braterman, P. S.: Isotopic fractionation
between Fe(III) and Fe(II) in aqueous solutions, *Earth Planet. Sci. Lett.*, 195, 141-153, 2002.
- Johnson, K. S., Gordon, R. M., and Coale, K. H.: What controls dissolved iron concentrations in the world ocean?,
Mar. Chem., 57, 137-161, 1997.
- Kiczka, M., Wiederhold, J. G., Frommer, J., Kraemer, S. M., Bourdon, B., and Kretzschmar, R.: Iron isotope



- 963 fractionation during proton- and ligand-promoted dissolution of primary phyllosilicates, *Geochim.*
- 964 *Cosmochim. Acta*, 74, 3112-3128, 2010.
- 965 König, D., Conway, T. M., Hamilton, D. S., and Tagliabue, A.: Surface Ocean Biogeochemistry Regulates the
- 966 Impact of Anthropogenic Aerosol Fe Deposition on the Cycling of Iron and Iron Isotopes in the North Pacific,
- 967 *Geophys. Res. Lett.*, 49, e2022GL098016, <https://doi.org/10.1029/2022GL098016>, 2022.
- 968 König, D., Conway, T. M., Ellwood, M. J., Homoky, W. B., and Tagliabue, A.: Constraints on the Cycling of Iron
- 969 Isotopes From a Global Ocean Model, *Glob. Biogeochem. Cycle*, 35, e2021GB006968, 2021.
- 970 Kubik, E., Moynier, F., Paquet, M., and Siebert, J.: Iron Isotopic Composition of Biological Standards Relevant
- 971 to Medical and Biological Applications, *Frontiers in Medicine*, 8, 696367, 10.3389/fmed.2021.696367, 2021.
- 972 Kumar, A., Sarin, M. M., and Srinivas, B.: Aerosol iron solubility over Bay of Bengal: Role of anthropogenic
- 973 sources and chemical processing, *Mar. Chem.*, 121, 167-175, 2010.
- 974 Kurisu, M. and Takahashi, Y.: Testing Iron Stable Isotope Ratios as a Signature of Biomass Burning, *Atmosphere*,
- 975 10, 76, doi: 10.3390/atmos10020076, 2019.
- 976 Kurisu, M., Adachi, K., Sakata, K., and Takahashi, Y.: Stable isotope ratios of combustion iron produced by
- 977 evaporation in a steel plant, *ACS Earth and Space Chem.*, 3, 588-598, 2019.
- 978 Kurisu, M., Takahashi, Y., Iizuka, T., and Uematsu, M.: Very low isotope ratio of iron in fine aerosols related to
- 979 its contribution to the surface ocean, *J. Geophys. Res.-Atmos.*, 121, 11119-11136, 2016a.
- 980 Kurisu, M., Sakata, K., Uematsu, M., Ito, A., and Takahashi, Y.: Contribution of combustion Fe in marine aerosols
- 981 over the northwestern Pacific estimated by Fe stable isotope ratios, *Atmos. Chem. Phys.*, 21, 16027-16050,
- 982 2021.
- 983 Kurisu, M., Sakata, K., Miyamoto, C., Takaku, Y., Iizuka, T., and Takahashi, Y.: Variation of Iron Isotope Ratios
- 984 in Anthropogenic Materials Emitted through Combustion Processes, *Chem. Lett.*, 45, 970-972, 2016b.
- 985 Kurisu, M., Sakata, K., Nishioka, J., Obata, H., Conway, T. M., Hunt, H. R., Sieber, M., Suzuki, K., Kashiwabara,
- 986 T., Kubo, S., Takada, M., and Takahashi, Y.: Source and fate of atmospheric iron supplied to the subarctic
- 987 North Pacific traced by stable iron isotope ratios, *Geochim. Cosmochim. Acta*, 378, 168-185, 2024.
- 988 Labatut, M., Lacan, F., Pradoux, C., Chmieleff, J., Radic, A., Murray, J. W., Poitrasson, F., Johansen, A. M., and
- 989 Thil, F.: Iron sources and dissolved-particulate interactions in the seawater of the Western Equatorial Pacific,
- 990 iron isotope perspectives, *Glob. Biogeochem. Cycle*, 28, 1044-1065, 2014.
- 991 Lacan, F., Radic, A., Jeandel, C., Poitrasson, F., Sarthou, G., Pradoux, C., and Freydisier, R.: Measurement of the
- 992 isotopic composition of dissolved iron in the open ocean, *Geophys. Res. Lett.*, 35, L24610,
- 993 doi:10.1029/2008GL035841, 2008.
- 994 Lacan, F., Radic, A., Labatut, M., Jeandel, C., Poitrasson, F., Sarthou, G., Pradoux, C., Chmieleff, J., and Freydisier,
- 995 R.: High-Precision Determination of the Isotopic Composition of Dissolved Iron in Iron Depleted Seawater
- 996 by Double Spike Multicollector-ICPMS, *Analytical Chemistry*, 82, 7103-7111, 2010.
- 997 Li, R., Zhang, H. H., Wang, F., He, Y. T., Huang, C. P., Luo, L., Dong, S. W., Jia, X. H., and Tang, M. J.: Mass
- 998 fractions, solubility, speciation and isotopic compositions of iron in coal and municipal waste fly ash, *Sci.*
- 999 *Total Environ.*, 838, 155974, 2022.
- 1000 Li, W. J., Xu, L., Liu, X. H., Zhang, J. C., Lin, Y. T., Yao, X. H., Gao, H. W., Zhang, D. Z., Chen, J. M., Wang, W.
- 1001 X., Harrison, R. M., Zhang, X. Y., Shao, L. Y., Fu, P. Q., Nenes, A., and Shi, Z. B.: Air pollution-aerosol
- 1002 interactions produce more bioavailable iron for ocean ecosystems, *Science Adv.*, 3, e1601749, 2017.
- 1003 Liu, L., Li, W., Lin, Q., Wang, Y., Zhang, J., Zhu, Y., Yuan, Q., Zhou, S., Zhang, D., Baldo, C., and Shi, Z.: Size-
- 1004 dependent aerosol iron solubility in an urban atmosphere, *NPJ Climate and Atmospheric Science*, 5, 53, 2022.
- 1005 Liu, M., Matsui, H., Hamilton, D. S., Rathod, S. D., Lamb, K. D., and Mahowald, N. M.: Representation of iron
- 1006 aerosol size distributions of anthropogenic emissions is critical in evaluating atmospheric soluble iron input
- 1007 to the ocean, *Atmos. Chem. Phys.*, 24, 13115-13127, 2024.
- 1008 Lobato, L. M., Figueiredo e Silva, R. C., Angerer, T., de Cássia Oliveira Mendes, M., and Hagemann, S. G.: Iron
- 1009 Isotopes Applied to BIF-Hosted Iron Deposits, in: *Isotopes in Economic Geology, Metallogenesis and*
- 1010 *Exploration*, edited by: Huston, D. and Gutzmer, J., Springer International Publishing, Cham, 399-432, 2023.
- 1011 Mahowald, N. M., Hamilton, D. S., Mackey, K. R. M., Moore, J. K., Baker, A. R., Scanza, R. A., and Zhang, Y.:
- 1012 Aerosol trace metal leaching and impacts on marine microorganisms, *Nature Comm.*, 9, 2614, 2018.
- 1013 Majestic, B. J., Anbar, A. D., and Herckes, P.: Elemental and iron isotopic composition of aerosols collected in a
- 1014 parking structure, *Sci. Total Environ.*, 407, 5104-5109, 2009a.
- 1015 Majestic, B. J., Anbar, A. D., and Herckes, P.: Stable Isotopes as a Tool to Apportion Atmospheric Iron, *Environ.*
- 1016 *Sci. Technol.*, 43, 4327-4333, 2009b.
- 1017 Marsay, C. M., Kadko, D., Landing, W. M., and Buck, C. S.: Bulk Aerosol Trace Element Concentrations and
- 1018 Deposition Fluxes During the U.S. GEOTRACES GP15 Pacific Meridional Transect, *Glob. Biogeochem.*
- 1019 *Cycle*, 36, e2021GB007122, 2022.
- 1020 Maters, E. C., Mulholland, D. S., Flament, P., de Jong, J., Mattielli, N., Deboudt, K., Dhont, G., and Bychkov, E.:
- 1021 Laboratory study of iron isotope fractionation during dissolution of mineral dust and industrial ash in
- 1022 simulated cloud water, *Chemosphere*, 299, 134472, 2022.



- 1023 Mead, C., Herckes, P., Majestic, B. J., and Anbar, A. D.: Source apportionment of aerosol iron in the marine
1024 environment using iron isotope analysis, *Geophys. Res. Lett.*, 40, 5722-5727, 2013.
- 1025 Meskhidze, N., Chameides, W. L., Nenes, A., and Chen, G.: Iron mobilization in mineral dust: Can anthropogenic
1026 SO₂ emissions affect ocean productivity?, *Geophys. Res. Lett.*, 30, 2085, 2003.
- 1027 Meskhidze, N., Volker, C., Al-Abadleh, H. A., Barbeau, K., Bressac, M., Buck, C., Bundy, R. M., Croot, P., Feng,
1028 Y., Ito, A., Johansen, A. M., Landing, W. M., Mao, J. Q., Myriokefalitakis, S., Ohnemus, D., Pasquier, B., and
1029 Ye, Y.: Perspective on identifying and characterizing the processes controlling iron speciation and residence
1030 time at the atmosphere-ocean interface, *Mar. Chem.*, 217, 103704, 2019.
- 1031 Moore, C. M., Mills, M. M., Arrigo, K. R., Berman-Frank, I., Bopp, L., Boyd, P. W., Galbraith, E. D., Geider, R.
1032 J., Guieu, C., Jaccard, S. L., Jickells, T. D., La Roche, J., Lenton, T. M., Mahowald, N. M., Maranon, E.,
1033 Marinov, I., Moore, J. K., Nakatsuka, T., Oeschies, A., Saito, M. A., Thingstad, T. F., Tsuda, A., and Ulloa, O.:
1034 Processes and patterns of oceanic nutrient limitation, *Nature Geosci.*, 6, 701-710, 2013.
- 1035 Mulholland, D. S., Flament, P., de Jong, J., Mattioli, N., Deboudt, K., Dhont, G., and Bychkov, E.: In-cloud
1036 processing as a possible source of isotopically light iron from anthropogenic aerosols: New insights from a
1037 laboratory study, *Atmos. Environ.*, 259, 118505, 2021.
- 1038 Myriokefalitakis, S., Daskalakis, N., Mihalopoulos, N., Baker, A. R., Nenes, A., and Kanakidou, M.: Changes in
1039 dissolved iron deposition to the oceans driven by human activity: a 3-D global modelling study,
1040 *Biogeosciences*, 12, 3973-3992, 2015.
- 1041 Oakes, M., Ingall, E. D., Lai, B., Shafer, M. M., Hays, M. D., Liu, Z. G., Russell, A. G., and Weber, R. J.: Iron
1042 Solubility Related to Particle Sulfur Content in Source Emission and Ambient Fine Particles, *Environ. Sci.*
1043 *Technol.*, 46, 6637-6644, 2012.
- 1044 Pinedo-González, P., Hawco, N. J., Bundy, R. M., Armbrust, E. V., Follows, M. J., Cael, B. B., White, A. E.,
1045 Ferrón, S., Karl, D. M., and John, S. G.: Anthropogenic Asian aerosols provide Fe to the North Pacific Ocean,
1046 *Proc. Natl. Acad. Sci. U.S.A.*, 117, 27862-27868, 2020.
- 1047 Poitrasson, F.: On the iron isotope homogeneity level of the continental crust, *Chem. Geol.*, 235, 195-200, 2006.
- 1048 Radic, A., Lacan, F., and Murray, J. W.: Iron isotopes in the seawater of the equatorial Pacific Ocean: New
1049 constraints for the oceanic iron cycle, *Earth Planet. Sci. Lett.*, 306, 1-10, 2011.
- 1050 Rathod, S. D., Hamilton, D. S., Mahowald, N. M., Klimont, Z., Corbett, J. J., and Bond, T. C.: A Mineralogy-
1051 Based Anthropogenic Combustion-Iron Emission Inventory, *J. Geophys. Res.-Atmos.*, 125, e2019JD032114,
1052 doi: 10.1029/2019JD032114, 2020.
- 1053 Sakata, K., Sakaguchi, A., Yamakawa, Y., Miyamoto, C., Kurisu, M., and Takahashi, Y.: Measurement report:
1054 Stoichiometry of dissolved iron and aluminum as an indicator of the factors controlling the fractional solubility
1055 of aerosol iron – results of the annual observations of size-fractionated aerosol particles in Japan, *Atmos.*
1056 *Chem. Phys.*, 23, 9815-9836, 2023.
- 1057 Sakata, K., Kurisu, M., Takeichi, Y., Sakaguchi, A., Tanimoto, H., Tamenori, Y., Matsuki, A., and Takahashi, Y.:
1058 Iron (Fe) speciation in size-fractionated aerosol particles in the Pacific Ocean: The role of organic
1059 complexation of Fe with humic-like substances in controlling Fe solubility, *Atmos. Chem. Phys.*, 22, 9461-
1060 9482, 2022.
- 1061 Schauble, E. A.: Applying stable isotope fractionation theory to new systems, in: *Geochemistry of Non-*
1062 *Traditional Stable Isotopes*, edited by: Johnson, C. M., Beard, B. L., and Albarede, F., *Reviews in Mineralogy*
1063 *& Geochemistry*, 65-111, 10.2138/gsrmg.55.1.65, 2004.
- 1064 Sedwick, P. N., Sholkovitz, E. R., and Church, T. M.: Impact of anthropogenic combustion emissions on the
1065 fractional solubility of aerosol iron: Evidence from the Sargasso Sea, *Geochem. Geophys. Geosyst.*, 8,
1066 Q10Q06, DOI: 10.1029/2007GC001586, 2007.
- 1067 Shelley, R. U., Morton, P. L., and Landing, W. M.: Elemental ratios and enrichment factors in aerosols from the
1068 US-GEOTRACES North Atlantic transects, *Deep Sea Research Part II: Topical Studies in Oceanography*, 116,
1069 262-272, 2015.
- 1070 Shi, Z. B., Krom, M. D., Jickells, T. D., Bonneville, S., Carslaw, K. S., Mihalopoulos, N., Baker, A. R., and
1071 Benning, L. G.: Impacts on iron solubility in the mineral dust by processes in the source region and the
1072 atmosphere: A review, *Aeolian Res.*, 5, 21-42, 2012.
- 1073 Shi, Z. B., Woodhouse, M. T., Carslaw, K. S., Krom, M. D., Mann, G. W., Baker, A. R., Savov, I., Fones, G. R.,
1074 Brooks, B., Drake, N., Jickells, T. D., and Benning, L. G.: Minor effect of physical size sorting on iron
1075 solubility of transported mineral dust, *Atmos. Chem. Phys.*, 11, 8459-8469, 2011.
- 1076 Sholkovitz, E. R., Sedwick, P. N., and Church, T. M.: Influence of anthropogenic combustion emissions on the
1077 deposition of soluble aerosol iron to the ocean: Empirical estimates for island sites in the North Atlantic,
1078 *Geochim. Cosmochim. Acta*, 73, 3981-4003, 2009.
- 1079 Sholkovitz, E. R., Sedwick, P. N., Church, T. M., Baker, A. R., and Powell, C. F.: Fractional solubility of aerosol
1080 iron: Synthesis of a global-scale data set, *Geochim. Cosmochim. Acta*, 89, 173-189, 2012.
- 1081 Sieber, M., Conway, T. M., de Souza, G. F., Hassler, C. S., Ellwood, M. J., and Vance, D.: Isotopic fingerprinting
1082 of biogeochemical processes and iron sources in the iron-limited surface Southern Ocean, *Earth and Planetary*



- 1083 Science Letters, 567, 116967, doi: 116910.111016/j.epsl.112021.116967, 2021.
- 1084 Skulan, J. L., Beard, B. L., and Johnson, C. M.: Kinetic and equilibrium Fe isotope fractionation between aqueous
- 1085 Fe(III) and hematite, *Geochim. Cosmochim. Acta*, 66, 2995-3015, 2002.
- 1086 Tagliabue, A., Bowie, A. R., Boyd, P. W., Buck, K. N., Johnson, K. S., and Saito, M. A.: The integral role of iron
- 1087 in ocean biogeochemistry, *Nature*, 543, 51-59, 2017.
- 1088 Waeles, M., Baker, A. R., Jickells, T., and Hoogewerff, J.: Global dust teleconnections: aerosol iron solubility and
- 1089 stable isotope composition, *Environ. Chem.*, 4, 233-237, 2007.
- 1090 Wang, Y., Wu, L., Hu, W., Li, W., Shi, Z., Harrison, R. M., and Fu, P.: Stable iron isotopic composition of
- 1091 atmospheric aerosols: An overview, *npj Climate and Atmospheric Science*, 5, 75, 10.1038/s41612-022-00299-
- 1092 7, 2022.
- 1093 Wei, T., Dong, Z., Zong, C., Liu, X., Kang, S., Yan, Y., and Ren, J.: Global-scale constraints on the origins of
- 1094 aerosol iron using stable iron isotopes: A review, *Earth-Sci. Rev.*, 258, 104943,
- 1095 <https://doi.org/10.1016/j.earscirev.2024.104943>, 2024.
- 1096 Welch, S. A., Beard, B. L., Johnson, C. M., and Braterman, P. S.: Kinetic and equilibrium Fe isotope fractionation
- 1097 between aqueous Fe(II) and Fe(III), *Geochim. Cosmochim. Acta*, 67, 4231-4250, 2003.
- 1098 Weyer, S. and Schwieters, J. B.: High precision Fe isotope measurements with high mass resolution MC-ICPMS,
- 1099 *Int. J. Mass Spectrom.*, 226, 355-368, 2003.
- 1100 Wiederhold, J. G., Kraemer, S. M., Teutsch, N., Borer, P. M., Halliday, A. N., and Kretzschmar, R.: Iron Isotope
- 1101 Fractionation during Proton-Promoted, Ligand-Controlled, and Reductive Dissolution of Goethite, *Environ.*
- 1102 *Sci. Technol.*, 40, 3787-3793, 2006.
- 1103 Xiao, C., Du, Z., Handley, M. J., Mayewski, P. A., Cao, J., Schüpbach, S., Zhang, T., Petit, J.-R., Li, C., Han, Y.,
- 1104 Li, Y., and Ren, J.: Iron in the NEEM ice core relative to Asian loess records over the last glacial–interglacial
- 1105 cycle, *National Science Review*, 8, nwaa144, 10.1093/nsr/nwaa144, 2020.
- 1106 Yin, N.-H., Louvat, P., Thibault-De-Chanvalon, A., Sebilo, M., and Amouroux, D.: Iron isotopic fractionation
- 1107 driven by low-temperature biogeochemical processes, *Chemosphere*, 316, 137802,
- 1108 <https://doi.org/10.1016/j.chemosphere.2023.137802>, 2023.
- 1109 Zhang, H. H., Li, R., Dong, S. W., Wang, F., Zhu, Y. J., Meng, H., Huang, C. P., Ren, Y., Wang, X. F., Hu, X. D.,
- 1110 Li, T. T., Peng, C., Zhang, G. H., Xue, L. K., Wang, X. M., and Tang, M. J.: Abundance and Fractional
- 1111 Solubility of Aerosol Iron During Winter at a Coastal City in Northern China: Similarities and Contrasts
- 1112 Between Fine and Coarse Particles, *J. Geophys. Res.-Atmos.*, 127, e2021JD036070, DOI:
- 1113 10.1029/2021JD036070, 2022.
- 1114 Zhang, H. H., Li, R., Huang, C. P., Li, X. F., Dong, S. W., Wang, F., Li, T. T., Chen, Y. Z., Zhang, G. H., Ren, Y.,
- 1115 Chen, Q. C., Huang, R. J., Chen, S. Y., Xue, T., Wang, X. M., and Tang, M. J.: Seasonal variation of aerosol
- 1116 iron solubility in coarse and fine particles at an inland city in northwestern China, *Atmos. Chem. Phys.*, 23,
- 1117 3543-3559, 2023.
- 1118 Zhang, T., Liu, J., Xiang, Y., Liu, X., Zhang, J., Zhang, L., Ying, Q., Wang, Y., Wang, Y., Chen, S., Chai, F., and
- 1119 Zheng, M.: Quantifying anthropogenic emission of iron in marine aerosol in the Northwest Pacific with
- 1120 shipborne online measurements, *Sci. Total Environ.*, 912, 169158,
- 1121 <https://doi.org/10.1016/j.scitotenv.2023.169158>, 2024.
- 1122 Zhu, C., Lu, W., He, Y., Ke, S., Wu, H., and Zhang, L.: Iron isotopic analyses of geological reference materials on
- 1123 MC-ICP-MS with instrumental mass bias corrected by three independent methods, *Acta Geochimica*, 37, 691-
- 1124 700, 2018.
- 1125 Zhu, Y., Li, W., Wang, Y., Zhang, J., Liu, L., Xu, L., Xu, J., Shi, J., Shao, L., Fu, P., Zhang, D., and Shi, Z.: Sources
- 1126 and processes of iron aerosols in a megacity in Eastern China, *Atmos. Chem. Phys.*, 22, 2191-2202, 2022.
- 1127 Zhu, Y. H., Li, W. J., Lin, Q. H., Yuan, Q., Liu, L., Zhang, J., Zhang, Y. X., Shao, L. Y., Niu, H. Y., Yang, S. S.,
- 1128 and Shi, Z. B.: Iron solubility in fine particles associated with secondary acidic aerosols in east China, *Environ.*
- 1129 *Pollut.*, 264, 114769, 2020.
- 1130 Zuo, P., Huang, Y., Liu, P., Zhang, J., Yang, H., Liu, L., Bi, J., Lu, D., Zhang, Q., Liu, Q., and Jiang, G.: Stable
- 1131 Iron Isotopic Signature Reveals Multiple Sources of Magnetic Particulate Matter in the 2021 Beijing
- 1132 Sandstorms, *Environ. Sci. Tech. Lett.*, 9, 299-305, 2022.
- 1133